Am J Cancer Res 2026;16(2):741-765
www.ajcr.us /ISSN:2156-6976/ajcr0170480

Original Article

Inhibition of RAB7 promotes CD8$^+$ T cell activation via the STING/IRF1/CCL5/CXCL10 signaling axis to promote PD-1-mediated anti-lung cancer efficacy

Xiaoli Liu[1], Zhiqiang Jiang[2], Ruijie Li[3], Jia Li[1], Lu Zhang[1], Huaimin Liu[1]

[1]Department of Integrated Traditional Chinese and Western Medicine, The Affiliated Cancer Hospital of Zhengzhou University and Henan Cancer Hospital, Zhengzhou 450008, Henan, China; [2]Department of General Surgery, The Affiliated Cancer Hospital of Zhengzhou University and Henan Cancer Hospital, Zhengzhou 450008, Henan, China; [3]Department of Medical Oncology, Henan Provincial Chest Hospital, Zhengzhou 450000, Henan, China

Received December 3, 2025; Accepted February 2, 2026; Epub February 25, 2026; Published February 28, 2026

Abstract: Programmed cell death protein 1 (PD-1) antibody is facing the challenge of drug resistance in cancer therapy. RAB7 plays a key role in autophagic lysosomal fusion, but its function in tumor immune regulation, especially whether it can enhance the efficacy of PD-1 inhibitors, is not clear. RAS-associated binding protein 7 (RAB7) and stimulator of interferon gene (STING) were knocked down by siRNA in lung squamous cell carcinoma (LUSC) cells. The effects of RAB7 and STING on the malignant phenotype of cells were evaluated. The autophagy flux and cytoplasmic double-stranded DNA (dsDNA) accumulation were observed by Western blot, RFP-GFP-LC3B tandem fluorescent probe, transmission electron microscopy and immunofluorescence. The expression of STING/interferon regulatory factor 1 (IRF1) pathway was analyzed by Western blot. CD8$^+$ T cells were co-cultured with lung cancer cells to investigate RAB7 knockdown effects on CD8$^+$ T cell activation. Finally, mouse subcutaneous xenograft models were established to explore RAB7 knockdown combined with anti-PD-1 treatment. RAB7 was highly expressed in lung cancer, and its knockdown blocked autophagy flux, leading to cytoplasmic dsDNA accumulation, which in turn activated the STING/IRF1 signaling axis and up-regulated C-C motif chemokine ligand 5 (CCL5) and C-X-C motif chemokine ligand (CXCL) 10. In the co-culture system, knockdown of RAB7 promoted CD8$^+$ T cell proliferation and cytotoxicity, up-regulated Perforin expressions, and decreased the levels of PD-1 and CD39. The combined application inhibited tumor growth, which was accompanied by activation of STING/IRF1 pathway, increased tumor infiltration and CD8$^+$ T cell function. STING knockdown reversed all anti-tumor and immune activation effects mediated by RAB7 knockdown. In summary, knockdown of RAB7 activated the STING/IRF1/CCL5/CXCL10 signaling pathway by blocking autophagy flux, enhanced the activation and infiltration of CD8$^+$ T cells, and significantly enhanced PD-1 antibody efficacy against lung cancer.

Keywords: RAS-associated binding protein 7, lung cancer, CD8$^+$ T cells, programmed cell death protein 1

Introduction

The number of global lung cancer cases and deaths in 2022 was 2.4803 million and 1.8172 million, respectively, ranking first among all malignant tumors [1]. Lung cancer incidence in China have shown a significant upward trend [2, 3]. The 5-year survival rate after distant metastasis of lung cancer is only about 5% [4, 5], and the disease burden is extremely serious. Studies have shown that programmed cell death protein-1 (PD-1) and programmed cell death ligand 1 (PD-L1) immunotherapy combined with cytotoxic chemotherapy drugs have a good effect on lung cancer [6]. The survival time of 16% patients with advanced squamous non-small cell lung cancer (NSCLC) and 15% patients with advanced non-squamous NSCLC is up to 5 years or longer [7, 8]. However, immunotherapy has limitations such as low response rate, susceptibility to drug resistance and immune-related adverse reactions. Therefore, how to improve the efficacy of immunotherapy is the focus of current cancer-related research.

Studies have shown that the efficacy of immunotherapy for lung cancer is strongly associated with tumor-infiltrating lymphocytes (TILs) func-

tion [9]. TILs are highly heterogeneous lymphocyte subsets that can infiltrate the cancer tissue after the immune response of the body. Through cancer cell identification and killing, the immune response is achieved, and less cytokine storm is generated [10]. The enhanced anti-tumor effect of TILs is mainly attributed to $CD8^+$ T lymphocyte reactivation, which inhibits cancer cell growth. Functional $CD8^+$ T cells can effectively remove tumor cells. However, $CD8^+$ T cell depletion occurs in tumor microenvironment (TME). They are usually an important reason for tumor immune escape and resistance to PD-L1 inhibitors [11]. When tumor cells produce cytoplasmic double-stranded DNA (dsDNA) due to genomic instability, replication stress or therapeutic damage, cyclic GMP-AMP synthase (cGAS) will sense these dsDNA and catalyze cGAMP production, which in turn stimulates stimulator of interferon gene (STING) protein on the endoplasmic reticulum [12-14]. Activated STING activates interferon regulatory factor (IRF) by phosphorylating TANK binding kinase 1 (TBK1). It drives interferon (IFN) and a variety of chemokines (such as C-C motif chemokine ligand 5 (CCL5), C-X-C motif chemokine ligand 9 (CXCL9), CXCL10) expressions to activate T cells and establish an anti-tumor immune response [15-17]. Therefore, exploring safe and effective strategies that can activate the STING signal axis is a feasible way to enhance the effect of immunotherapy.

Autophagy is the core process for cells to maintain their homeostasis. It degrades intracellular damaged organelles and proteins by forming autophagosome-lysosome structures. However, autophagy plays a complex 'double-edged sword' role in tumors. On the one hand, autophagy can inhibit tumorigenesis; on the other hand, established tumors use autophagy to cope with various stresses and maintain their survival and proliferation [18, 19]. It is particularly noteworthy that there is a close and complex interaction between the autophagy pathway and innate immune signals. There is evidence that autophagy can selectively degrade dsDNA or cGAS, STING and other signaling molecules in cytoplasm, thus negatively regulating cGAS-STING axis [20, 21]. This suggests that intervention in specific aspects of autophagic flux may be a potential means to release immunogenic signals from the inside and break the state of immune tolerance. RAS-associated binding protein 7 (RAB7) is a small guanosine triphosphatase (GTPase), which is mainly present in late endosomes and controls autophagy, transport and migration of cells. RAB7 has both carcinogenic and anti-cancer effects [22]. Moreover, RAB7 protein, as a transporter, is a key membrane protein on lysosomes and a core molecule regulating the late stage of autophagic flux, and is vital for the maturation of autophagosomes [23]. RAB7 is highly expressed in cancer tissues, inhibition of RAB7 expression can prevent tumor growth *in vivo* [24]. RAB7A is overexpressed in pancreatic cancer tissues and is a risk factor affecting patient prognosis [25]. Inhibition of RAB7 activity also inhibited tumor progression and autophagy flux in colorectal cancer [23]. Although RAB7's roles in tumor cell multiplication have been sporadically reported, there is still a lack of systematic research on its role in tumor immune regulation, especially in affecting STING signaling and $CD8^+$ T cell function by regulating autophagy flow.

The purpose of this study was to systematically elucidate whether and how inhibition of RAB7 promotes anti-PD-1 therapeutic efficacy through the STING/IRF1/CCL5/CXCL10 signaling axis. We explored the regulatory effect of knockdown of RAB7 alone or in combination with anti-PD-1 immunotherapy on the immune function of tumor-infiltrating $CD8^+$ T lymphocytes in lung cancer, and explored the internal mechanism, in order to provide reference for further combined treatment of lung cancer.

Methods

Correlation analysis

Tumor Immune Estimation Resource (TIMER) (http://timer.comp-genomics.org/) was used to infer the abundance of tumor-infiltrating immune cells from gene expression profiles. The correlation between RAB7 and immune subtypes was analyzed by TISIDB (http://cis.hku.hk/TISIDB/).

Cell grouping and transfection

Human normal lung bronchial epithelial cells Beas-2B and lung squamous cell carcinoma (LUSC) cell lines (NCI-H520, SK-MES-1, HCC-827 and NCI-H226) were purchased from SUNNCELL (Wuhan, China, SNL-203, SNL-394,

SNL-438, SNL-210, SNL-388). The cells were cultured in RPMI 1640 medium (SNM-001E, SUNNCELL) containing 10% fetal bovine serum (FBS) and 1% penicillin-streptomycin solution at 37°C in a 5% CO_2 cell incubator (Galaxy® 170 R, Eppendorf, Hamburg, Germany).

siRAB7 (5'-GGCAGUGACUUUCUUGGAUTT-3'), siSTING (5'-UCAUAAACUUUGGAUGCUA-3') and siNC (5'-GUGUCACGUTT-3') were purchased from Jinkairui Bioengineering Co., Ltd. (Wuhan, China). NCI-H520 and SK-MES-1 cells (1×10^5 cells/well) were seeded, and 70% confluence was achieved after 24 h. The above vectors were transfected into cells according to the LipofectamineTM 3000 (L3000001, Invitrogen, USA) instructions. Each well was diluted with 50 nmol/L siRNA and 7.5 μL Lipofectamine 3000 in 250 μL Opti-MEM, respectively. After standing for 5 min, the mixture was incubated for 15 min to form a complex. The complex was added drop by drop into the well, replaced with complete medium after 6 h, and cultured for 48 h. Then the knockdown efficiencies were detected.

The transfected LUSC cells were cultured for 24, 48, 72 and 96 h, respectively, and 10 μL of cell counting kit-8 (CCK-8) working solution (SNK-010, SUNNCELL) was added and incubated in dark for 2 h. The optical density (OD) values of the cells in each group at 450 nm were measured by a microplate reader (Cytation 5, Agilent, California, USA) to evaluate cell viability.

Plate clone formation experiment

NCI-H520 and SK-MES-1 cells were digested and resuspended into a single cell suspension. The cells were inoculated into 6-well plates, and cultured at 37°C in a 5% CO_2 incubator for 10-14 days until a cell colony with a diameter greater than 50 μm was visible to the naked eye under a microscope (BX53, Olympus, Tokyo, Japan). At the end of culture, the culture medium was discarded, and the cell colonies were fixed with 4% paraformaldehyde (P0099, Beyotime, Shanghai, China) for 20 min, and then stained with 0.1% crystal violet solution (C0121, Beyotime) for 5 min. Finally, the excess dye was gently washed with running water and culture dish was dried. Observe the cell colony (usually defined as a colony with a population of more than 50 cells), count and take photos.

Cell scratch test

NCI-H520 and SK-MES-1 cells were cultured in 6-well plates. The 100 μL pipette tip was used to scratch the bottom of the vertical orifice plate in a straight line. The migration of cells was observed under a microscope at 0 and 12 h after culture, and the relative migration rate of cells in each group was measured and recorded by Image J software.

Autophagic flux detection

RFP-GFP-LC3 was used to construct an autophagy dual fluorescent plasmid to evaluate autophagic flux. RFP-GFP-LC3 (HANBIO, Shanghai, China) was transfected in 6-well plates with LipofectamineTM 3000 for 24 h. After transfection with siRAB7 and siNC, the cells were fixed with 4% paraformaldehyde, and then sealed with an anti-fluorescence quencher. Fluorescence microscopy (Axio Observer 3, Zeiss, Oberkohen, Germany) was used to detect the autophagic compartment. Six fields of view were chosen from each dish to confirm GFP-LC3 and RFP-LC3 fluorescence point number, thereby quantifying the level of autophagy flux.

Transmission electron microscope (TEM)

LUSC cells were slowly added with precooled 2.5% glutaraldehyde and stored at 4°C overnight. Immobilize with 1% UO_4 for 1.5 h at 4°C and wash with PBS for 3 times. The cells were dehydrated by gradient concentration of ethanol, and finally treated with anhydrous acetone for 20 min. Cells were placed overnight in epoxy resin Ep812 (GP2001, Servicebio, Wuhan, China). The samples were cut into 80 nm-thick sections using an ultra-thin slicing machine and stained with uranium acetate and lead citrate for 5 min. Finally, transmission electron microscopy (JEM1400, Jeol, Tokyo, Japan) was used to observe the autophagic structure.

Detection of dsDNA by Picogreen method

The dsDNA content in LUSC cells was detected according to the instructions of PicoGreen dsDNA fluorescence quantitative assay kit (P7581, Thermo Fisher, Massachusetts, USA). After the treatment of NCI-H520 and SK-MES-1 cells, the cell lysate was added, the cell membrane was lysed on ice, and the supernatant was collected after centrifugation. Standard samples were prepared at concentrations of

1000, 100, 25, 10, 2.5, and 0.25 ng/mL, and the cell supernatant samples were diluted. 100 μL was added, and 100 μL of diluted PicoGreen working solution was added. Mix well and avoid light for 3 min. The signal intensity was detected by a fluorescence microplate reader. The dsDNA levels were calculated.

Cell co-culture

10 mL human peripheral blood was taken from healthy people in Zhengzhou University Cancer Hospital (Henan Cancer Hospital) and informed consent was obtained. 10 mL peripheral blood of healthy blood donors was collected in anticoagulant tubes and diluted with RPMI 1640 in a ratio of 1:2. A 15 mL centrifuge tube was taken out and 3 mL Ficocll solution was added. The diluted peripheral blood was slowly added along the tube wall. Peripheral blood mononuclear cells (PBMCs) were isolated by Ficoll density gradient centrifugation. According to the $CD8^+$ T cell sorting kit (480012, Biolegend, USA), $CD8^+$ T cell magnetic beads (130-045-201, Miltenyi Biotech, Germany) were added to PBMCs and incubated for 30 min. The cells were placed on a magnetic frame and allowed to stand for 10 min. The supernatant was discarded and resuspended in RPMI 1640 medium containing 10% FBS and 10 IU/mL interleukin (IL)-2. The cells were seeded in 6-well plates coated with anti-CD3 (2.5 μg/mL) and anti-CD28 (2 μg/mL) antibodies [26] and cultured to initiate and maintain $CD8^+$ T cell activation and proliferation. Then NCI-H520 and SK-MES-1 cells were co-cultured with activated $CD8^+$ T cells at a ratio of 1:3.

The spleens of OT-I mice (whose $CD8^+$ T cells specifically recognize the Ovalbumin (OVA) peptide SIINFEKL) were removed under sterile conditions, ground and prepared into single cell suspension through a 70 μm cell sieve. After removing red blood cells using red blood cell lysate (420301, BioLegend), mouse $CD8^+$ T cell sorting kit (480008, BioLegend) was used to obtain $CD8^+$ T cells in strict accordance with the instructions. The cells were activated in RPMI 1640 medium containing 10% FBS, CD3 (5 μg/mL) and CD28 (2 μg/mL), and cultured in a cell incubator at 37°C and 5% CO_2 for 36 h [27]. Subsequently, activated $CD8^+$ T cells were co-cultured with different proportions of tumor cells (5:1, 10:1, 15:1 and 20:1). After 24 h, $CD8^+$ T cells were taken out and the plate was washed three times with PBS. The apoptosis of tumor cells was evaluated by flow cytometry, and the survival rate of tumor cells was evaluated by CCK-8 assay.

UN-SCC679-OVA cells transfected with shNC, shRAB7 or shRAB7+shSTING plasmids were incubated with SIINFEKL-H-2Kb antibody (αH-2Kb, 141604, BioLegend) or IgG control antibody (100 μg/mL) for 30 min at 4°C. Subsequently, activated OT-I $CD8^+$ T cells were co-cultured with tumor cells at a ratio of 5:1, and the cytotoxicity of OT-I $CD8^+$ T cells was evaluated by flow cytometry.

Carboxyfluorescein succinimidyl ester (CFSE)

$CD8^+$ T cells (1×10^6 cells/mL) were resuspended in PBS. Carboxyfluorescein succinimidyl ester (CFSE) working solution was added to a final concentration of 5 μM and incubated in dark for 20 min. Subsequently, 5-fold volume of pre-cooled medium was immediately added to terminate labeling. Then, these $CD8^+$ T cells were co-cultured. After culture, $CD8^+$ T cell was collected and incubated with CD8 (ab237709, Abcam, Cambridge, UK) flow antibody for 30 min. Cells were resuspended and $CD8^+$ T cell proliferation level was measured using flow cytometry.

Lactate dehydrogenase (LDH) assay

$CD8^+$ T cell cytotoxicity was tested using LDH kits (C20301, Thermo Fisher). The co-cultured cell culture medium was collected, centrifuged for 10 min, 100 μL supernatant was taken, and 60 μL LDH detection solution was added for incubation in dark for 30 min. The $OD_{490\ nm}$ values were read using a microplate reader. Cytotoxicity (%) = (reaction pore $OD_{490\ nm}$-natural release pore $OD_{490\ nm}$)/(maximum release pore $OD_{490\ nm}$-natural release pore $OD_{490\ nm}$) × 100% [28].

Transwell experiment

Matrigel was thawed overnight at 4°C, placed on an ice table, mixed with pre-cooled medium at a ratio of 1:8, and set aside. 60 μL Matrigel was added vertically and evenly to the upper chamber to avoid bubbles and adherence. After incubation for 1 h, the matrix gel was discarded and the remaining liquid in the upper chamber

was discarded. The medium was added to each well in the upper and lower chambers, and the membrane was hydrated after 2 h of culture. LUSC cells were taken and adjusted to a density of 2.5×10^5 cells/mL with serum-free medium, and 150 μL was added to the upper chamber. A total of 600 μL of complete medium containing 20% FBS was added to the lower chamber. After 48 h of culture, the upper and lower chambers were discarded. After washing with PBS buffer for 2 times, 4% paraformaldehyde was added and fixed for 15 min. The cells were washed twice with PBS buffer, stained with 0.1% crystal violet for 30 min, and rinsed with PBS buffer for 3 times. The non-invasive cells and Matrigel in the upper chamber were gently wiped off with cotton swabs. Six regions were randomly selected and photographed under a microscope to count the number of invasive cells.

At the same time, Transwell assay was used to detect $CD8^+$ T cells penetrating the membrane. NCI-H520 and SK-MES-1 cells were added to the lower chamber, and $CD8^+$ T cells were added to the upper chamber, and incubated for 4 h. The remaining steps were the same as the invasion experiment. Finally, the number of migrations to the lower room is counted.

Mice grouping and intervention

All animal experiments were approved by the Henan Cancer Hospital Ethics Committee (Approval No. 2022-KY-0151-001). Female SPF grade C57BL/6 mice, 6-8 weeks of age, weighing 18-22 g, purchased from Sberfos Biotechnology Co., Ltd. (Beijing, China). All mice were housed in an SPF animal room with 22°C and 50% relative humidity to simulate normal circadian rhythms. Mice can eat and drink freely.

The mice were randomly divided into 4 groups: shCtrl group, anti-PD-1+shCtrl group, shRAB7 group and anti-PD-1+shRAB7 group. Mice in the shCtrl and anti-PD-1+shCtrl groups were subcutaneously injected with 1×10^6 UN-SCC-679 cells (mouse origin, RC-T2571, YaJi Biological, Shanghai, China) transfected with shCtrl, and the remaining mice were subcutaneously injected with 1×10^6 UN-SCC679 cells transfected with shRAB7. Mice in the anti-PD-1 intervention group were intraperitoneally injected with 10 mg/kg anti-PD-1 on days 11, 14, 17, 20, and 23 (BE0146, BioXcell, New Hampshire, USA). During this period, the body weight and tumor diameter of the mice were measured every 5 days, and the tumor volume (1/2 × long diameter × short diameter^2, mm^3) was calculated. After 25 days, the mice in each group were weighed and recorded by electronic balance. Then all mice were anesthetized by inhalation of 5% isoflurane, and subsequently euthanized by cervical dislocation. The tumor tissues were collected and weighed on an electronic balance. Some tumor tissues were immersed in 4% paraformaldehyde for fixation. Another part of the tumor tissue was stored at -80°C.

Immunohistochemistry

The fixed tumor tissue was dehydrated with gradient ethanol, transparent with xylene, and embedded in paraffin. The tissue was serially sectioned on a microtome (RM2255, Leica, Wetzlar, Germany) with a thickness of about 5 μm. After the paraffin section of the tumor tissue was baked, xylene was dewaxed and gradient ethanol was hydrated. Endogenous peroxidase was inhibited by incubation with 3% H_2O_2 for 20 min in the dark. The slices were placed in sodium citrate-citrate buffer. The slices were heated to above 95°C by microwave oven and kept at high temperature for 20 min, then removed and cooled to room temperature naturally. Add Ki67 (ab279657, 1:500, Abcam) primary antibody, 4°C refrigerator overnight. The first antibody was discarded, PBS was washed, the second antibody (ab6728, 1:2000, Abcam) was added and incubated for 2 h, PBS rinsed, DAB coloration, hematoxylin nuclear re-staining. Gradient ethanol dehydration, xylene transparent after sealing. Six fields of view were randomly selected under the microscope to take photos and perform data statistics.

TUNEL staining

Paraffin sections of tumor tissues were subjected to dewaxing to water, protease K repair antigen without DNase, and membrane rupture. TUNEL reaction solution (G1504, Servicebio) was prepared and added to the slice, and the TUNEL reaction solution was incubated for 1 h. After washing with PBS, DAPI was added for 10 min. The staining was observed under a fluorescence microscope and the image was taken. Six fields of vision were chosen, and the

average optical density value of apoptotic cells was recorded by Image J software.

Immunofluorescence

LUSC cells in each group were fixed with 4% paraformaldehyde, stained with PicoGreen dsDNA fluorescent reagent, and examined by fluorescence microscope. The cells and mouse tumor tissues were fixed with 4% paraformaldehyde and blocked with 10% goat serum for 30 min. Lysosomal-associated membrane protein 1 (LAMP1, ab25630, 1:500, Abcam), microtubule-light chain 3 beta (LC3B, ab48394, 1:500, Abcam), GFP (ab183734, 1:500, Abcam), phosphorylation of histone H2AX (γ-H2AX, 2577, 1:1000, Cell Signaling Technology, Massachusetts, USA), RAB7 (ab137029, 1:500, Abcam) and CD8 (ab316778, 1:100, Abcam) antibodies were added and incubated overnight at 4°C. After that, fluorescent antibody IgG and DAPI staining solution were added and incubated for 2 h and 10 min, respectively. The slides were dried and sealed with anti-fluorescence quencher. The slides were observed under a fluorescence microscope and the images were collected. The protein fluorescence intensity was analyzed by Image J software.

NCI-H520 and SK-MES-1 cells were incubated with 200 nM Mito-Tracker Red CMXRos (C1035, Beyotime) at 37°C for 15 min to specifically label the mitochondria of living cells. After staining, the cells were fixed with 4% paraformaldehyde at room temperature for 15 min and permeabilized with 0.1% Triton X-100 for 10 min. Then dsDNA antibody (76651, Cell Signaling Technology) was added and incubated at 4°C overnight. Fluorescent antibody IgG was added for incubation at room temperature for 2 h, and DAPI was used for nuclear restaining. The co-localization of dsDNA and mitochondria was observed under a fluorescence microscope.

Flow cytometry experiments

LUSC cells (1×10^5 cells) in each group and LUSC cells in the co-culture system were taken and placed in a flow tube. Each tube was added with 5 μL PI and 5 μL Annexin V-APC (E-CK-A217, Elabscience, Wuhan, China), incubated in the dark for 15 min, washed once, and resuspended with 500 μL phosphate buffer. Apoptosis was detected on a flow cytometer (FACSCelesta, BD Biosciences, USA).

The mouse tumor tissue was cut into pieces and digested with a digestive solution containing collagenase IV (1 mg/mL) at 37°C for 1 h to obtain a single cell suspension. Subsequently, the suspension was filtered using a cell sieve and tumor-infiltrating lymphocytes were enriched by Percoll method. The obtained cells were stained with CD8 and CD3 antibodies and incubated at 4°C in dark for 30 min. After staining, flow cytometry was used to collect data and calculate the percentage of $CD8^+$ T cells.

Western blot

The tumor tissues of mice were quickly thawed, and LUSC cells in each group were collected. RIPA lysis buffer containing protease inhibitor (P0013B, Beyotime) was added for homogenization. After lysis and centrifugation, the supernatant was the total protein. Then the protein was quantified by BCA kit (P0010, Beyotime), and the corresponding loading amount was calculated. After protein denaturation, SDS-PAGE gel was prepared. After gel electrophoresis separation, the protein was transferred to PVDF membrane, and the membrane was transferred for 60 min at a constant current of 250 mA at 4°C. The PVDF membrane was blocked with blocking solution (5% skim milk powder) for 90 min, incubated with primary antibody (**Table 1**), and slowly shaken overnight in a refrigerator at 4°C. The bands were incubated with the secondary antibodies of the corresponding species for 2 h, and the ECL luminescent chromogenic solution (P0018M, Beyotime) was added dropwise. The gel imaging system (Azure 600, Azure Biosystems, California, United States) was used to take pictures. The gray value of the protein bands was analyzed by ImageJ software, and the expression levels of different proteins were calculated.

Enzyme-linked immunosorbent assay (ELISA)

The cGAS ELISA kit was purchased from SYBIO (SY-H06146, Shanghai, China). The cells were collected, and the lysate was added. The cells were lysed on ice for 30 min, centrifuged at 4°C and 12000 r/min for 15 min, and the supernatant was collected as the sample to be tested. ELISA kits for mouse GZMB, IFN-γ and TNF-α were purchased from eBioscience (E-EL-M0594, E-EL-M0048, E-EL-M3063, Wuhan, China). The culture supernatant in the co-culture system was collected as the sample

Table 1. The primary antibodies used for Western blot

Protein name	Dilution ratio	Catalog number	Producer
RAS-associated binding protein 7 (RAB7)	1:10000	ab137029	Abcam
Microtubule-light chain 3 Beta (LC3B)	1:1000	M186-3	MBL
p62	1:50000	ab109012	Abcam
Perforin	1:1000	ab261727	Abcam
Interferon (IFN)-γ	1:2000	DF6045	Affinity
Granzyme B (GZMB)	1:1000	ab255868	Abcam
CD39	1:1000	ab223842	Abcam
Programmed cell death protein 1 (PD-1)	1:2000	DF2943	Affinity
phosphorylation of histone H2AX (γ-H2AX)	1:1000	2577	Cell Signaling Technology
Stimulator of interferon gene (STING)	1:2000	DF12090	Affinity
p-STING	1:1000	ab324229	Abcam
Interferon regulatory factor 1 (IRF1)	1:1000	ab230652	Abcam
C-C motif chemokine ligand 5 (CCL5)	1:2000	AF5151	Affinity
Cyclic GMP-AMP synthase (cGAS)	1:1000	ab224144	Abcam
C-X-C motif chemokine ligand 10 (CXCL10)	1:2000	DF6417	Affinity
GAPDH	1:10000	ab181602	Abcam

to be tested. The experiment was carried out in strict accordance with the operating instructions of the kit. The $OD_{450\ nm}$ value of each hole was detected by microplate reader. The standard curve was drawn according to the concentration and OD value of the standard, and the contents of cGAMP, GZMB, IFN-γ and TNF-α in each sample were calculated.

Detection of mitochondrial membrane potential (MMP)

NCI-H520 and SK-MES-1 cells in each group were collected, added with 1 mL JC-1 staining solution (C2003S, Beyotime), and incubated in a 5% CO_2 incubator at 37°C for 20 min. After the incubation was completed, the cells were washed twice with pre-cooled PBS to remove the free dye. Finally, the cells were resuspended with 500 μL PBS and immediately analyzed by flow cytometry.

Detection of reactive oxygen species (ROS)

NCI-H520 and SK-MES-1 cells were collected and resuspended in PBS containing 10 μM DCFH-DA fluorescent probe (S1105S, Beyotime). The cells were incubated at 37°C for 20 min in the dark. During the incubation period, the dye was gently shaken every 5 minutes to ensure full contact with the cells. After incubation, the cells were resuspended in PBS and immediately analyzed by flow cytometry to detect the relative level of ROS in the cells.

Detection of mitochondrial reactive oxygen species (mtROS)

After treatment of NCI-H520 and SK-MES-1 cells, MitoSOX Red probe (S0061S, Beyotime) diluted to 5 μM with serum-free medium was added and incubated at 37°C in dark for 20 min. After incubation, the cells were fixed with 4% paraformaldehyde for 15 min. After washing with PBS, DAPI staining solution was added for nuclear re-staining. Finally, the red fluorescence signal was observed and collected by fluorescence microscope.

Statistical analysis

Statistical analysis was conducted using SPSS version 27.0. Normality and homogeneity of variance were assessed for all data sets. For the comparison between the two groups, Student's t-test was used. One-way ANOVA was utilized, followed by Tukey's post hoc test for group comparisons. Repeated measures ANOVA was used for data comparison involving continuous time points (such as tumor volume or cell viability at different time points). Data for each group were presented as mean ± standard deviation, with $P < 0.05$ deemed statistically significant.

Results

Knockdown of RAB7 blocked autophagic flux and inhibited malignant phenotype of lung cancer cells

RAB7 protein has a cancer-promoting function, involving autophagy, apoptosis and cell migration [22]. RAB7 protein was elevated in a variety of LUSC cells (NCI-H520, SK-MES-1, HCC827 and NCI-H226) compared with Beas-2B cells, and it was highest in NCI-H520 and SK-MES-1 cells (**Figure 1A**, **1B**), so these two cells were selected for functional studies. After that, siRAB7 and siNC were transfected into LUSC cells, and the level of RAB7 protein in cells transfected with siRAB7 was significantly decreased, indicating that siRNA successfully knocked down RAB7 (**Figure 1C**, **1D**). Knockdown of RAB7 significantly lessened the cell viability (**Figure 1E**, **1F**), cell colony number, and the colony formation ability of LUSC cells (**Figure 1G**, **1H**), suggesting that knockdown of RAB7 suppressed LUSC cell proliferation. Knockdown of RAB7 also resulted in apoptotic cells (**Figure 1I**, **1J**), and cell migration rate (**Figure 1K**, **1L**) and the number of invasive cells (**Figure 1M**, **1N**) were also much lower than those of LUSC cells. Knockdown of RAB7 inhibited LUSC cell malignant phenotype.

RAB7 is strongly associated with autophagy [23] and is crucial for the maturation of autophagosomes. RAB7 knockdown resulted in an increase in p62 protein levels and an increase in LC3B-II/I protein ratio (**Figure 1O**, **1P**). RFP-GFP-LC3 can monitor autophagy flux. When autophagosomes fuse with lysosomes, GFP (green) fluorescence is quenched due to the acidic environment in lysosomes, while RFP (red) signal persists. RAB7 knockdown significantly increased the number of yellow fluorescent dots (**Figure 1Q**, **1R**), suggesting that autophagosomes accumulated but degradation was blocked, indicating impaired autophagy flux. TEM observed that in RAB7 knockdown cells, the number of undegraded autophagosomes in the cells was accumulated, but the number of mature autolysosomes that were undergoing degradation was rare (**Figure 1S**, **1T**). At the same time, immunofluorescence co-localization analysis of GFP-LC3B and LAMP1 showed that autophagosomes (GFP-LC3 fluorescent spots) in RAB7 knockdown cells was much higher than that in LUSC cells, but the co-localization of autophagosomes and lysosomes (i.e., autolysosomes) was reduced (**Figure 1U-W**). These results together indicated that RAB7 maintained autophagy flux by promoting autophagic lysosomes in lung cancer. RAB7 knockdown could block the autophagy process, and its mechanism involved reduced autophagosome maturation and impaired lysosomal function.

Knockdown of RAB7 promoted the accumulation of cytoplasmic dsDNA in lung cancer cells

RAB7 is an autophagy-related gene, and autophagy is closely related to dsDNA. To investigate whether RAB7 knockdown causes DNA damage and dsDNA accumulation in LUSC cells, we detected the expression level of DNA damage marker γ-H2AX and cytoplasmic dsDNA level. In RAB7 knockdown NCI-H520 and SK-MES-1 cells, the level of DNA damage marker γ-H2AX protein and positive cell number were markedly enhanced (**Figure 2A-D**), and cytoplasmic dsDNA level (**Figure 2E**) and fluorescence intensity (**Figure 2F**, **2G**) were also enhanced. Knockdown of RAB7 resulted in obvious DNA damage and cytoplasmic dsDNA accumulation. To further elucidate the upstream mechanism of dsDNA accumulation induced by autophagic flux blockade, we evaluated mitochondrial function. The results showed that the MMP of RAB7 knockdown cells was significantly decreased (**Figure 2H**, **2I**). In addition, we evaluated ROS and mtROS levels by DCFH-DA flow cytometry and MitoSOX Red staining. The intracellular ROS level (**Figure 2J**, **2K**) and mtROS content (**Figure 2L**, **2M**) of RAB7 knockdown cells were much higher than those of LUSC cells. These data suggested that RAB7 knockdown induced severe mitochondrial dysfunction and oxidative stress. Mitochondria were a potentially important source of cytoplasmic dsDNA. Subsequently, we observed the complete mtDNA structure by staining with dsDNA antibody. The results of immunofluorescence co-localization analysis of mitochondria and dsDNA showed that a large number of green fluorescence signals (dsDNA antibody labeling) and red fluorescence signals (MitoTracker labeled mitochondria) were clearly co-localized in RAB7 knockdown cells (**Figure 2N**, **2O**), suggesting that the leaked mtDNA was one of the main sources of cytoplasmic dsDNA

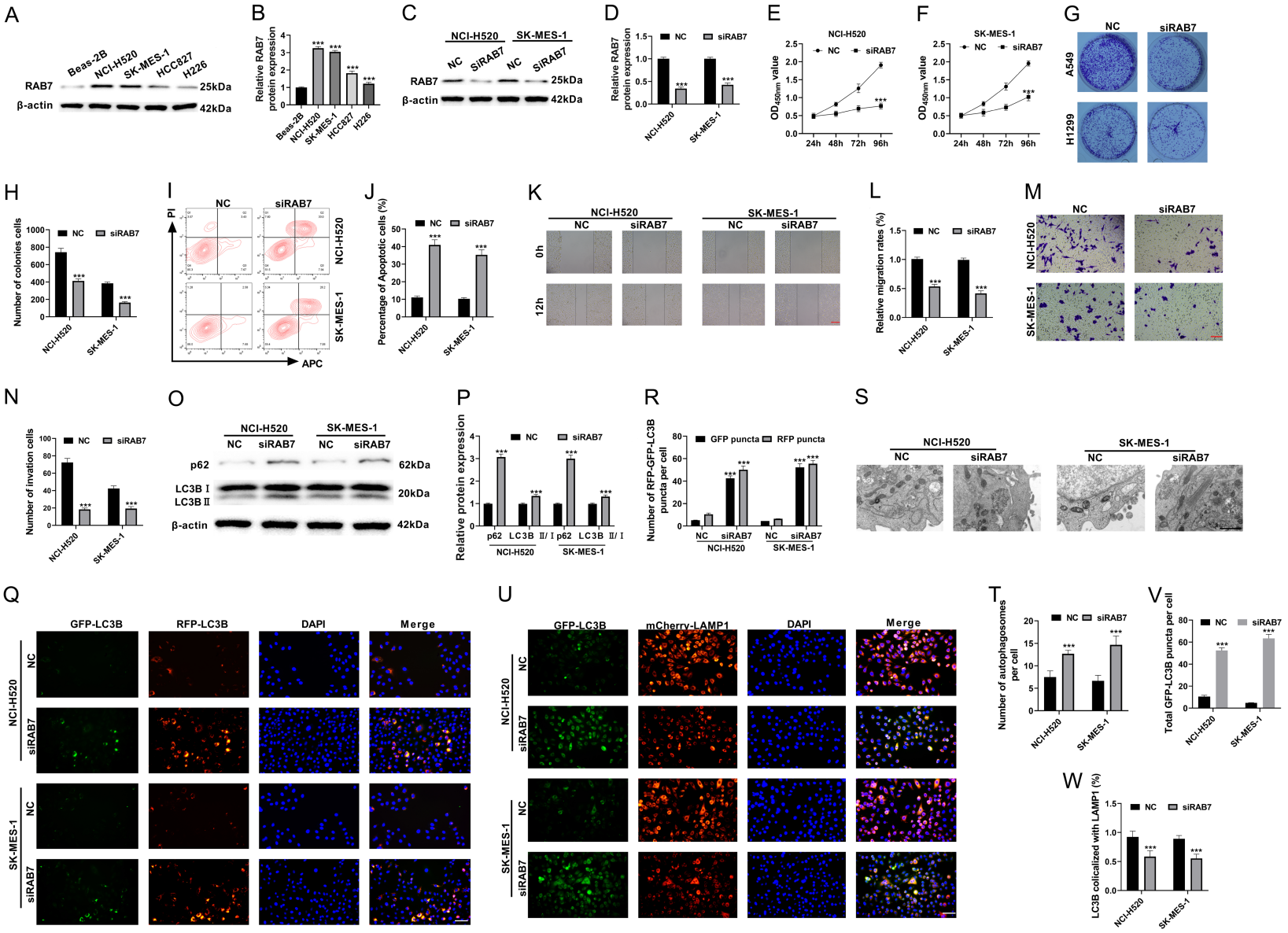
A
Beas-2B
NCI-H520
SK-MES-1
HCC827
H226
RAB7
β-actin
25kDa
42kDa
B
Relative RAB7 protein expression
C
NCI-H520
SK-MES-1
NC
siRAB7
D
Relative RAB7 protein expression
E
NCI-H520
OD450nm value
24h 48h 72h 96h
F
SK-MES-1
G
A549
H1299
H
Number of colonies cells
I
PI
APC
J
Percentage of Apoptotic cells (%)
K
0h
12h
L
Relative migration rates (%)
M
N
Number of invation cells
O
p62
LC3B Ⅰ
LC3B Ⅱ
62kDa
20kDa
P
Relative protein expression
R
GFP puncta
RFP puncta
Number of RFP-GFP-LC3B puncta per cell
S
Q
GFP-LC3B
RFP-LC3B
DAPI
Merge
U
mCherry-LAMP1
T
Number of autophagosomes per cell
V
Total GFP-LC3B puncta per cell
W
LC3B colicalized with LAMP1 (%)

Figure 1. Knockdown of RAB7 blocked autophagic flux and inhibited malignant phenotype of lung cancer cells. A, B. Western blot detected RAB7 protein in human bronchial epithelial cells Beas-2B and LUSC cell lines (NCI-H520, SK-MES-1, HCC827 and NCI-H226). C, D. RAB7 protein in LUSC cells was knocked down by siRNA, and the knockdown efficiency was analyzed. E, F. CCK-8 assays detected LUSC cell viability. G, H. LUSC cell proliferation ability was observed through plate colony formation assay. I, J. Flow cytometry analyzed LUSC cell apoptosis. K, L. Cell scratch assays detected LUSC cell migration (×10, 200 μm). M, N. Transwell assays detected LUSC cell invasion (×20, 100 μm). O, P. Western blot detected autophagy-related protein (p62, LC3B-I, and LC3B-II) levels. Q, R. RFP-GFP-LC3 was used to monitor autophagy flux (×40, 50 μm). S, T. The structure of autophagy was observed by TEM (×15.0 k, 1 μm). U-W. Immunofluorescence co-localization of GFP-LC3B and LAMP1 was used to analyze autophagy flux (×40, 50 μm). ***$P < 0.001$ *vs* NC group. Notes: RAB7, RAS-associated binding protein 7; LUSC, lung squamous cell carcinoma; CCK-8, cell counting kit-8; LC3B, microtubule-light chain 3 Beta; TEM, transmission electron microscope; LAMP1, lysosomal-associated membrane protein 1.

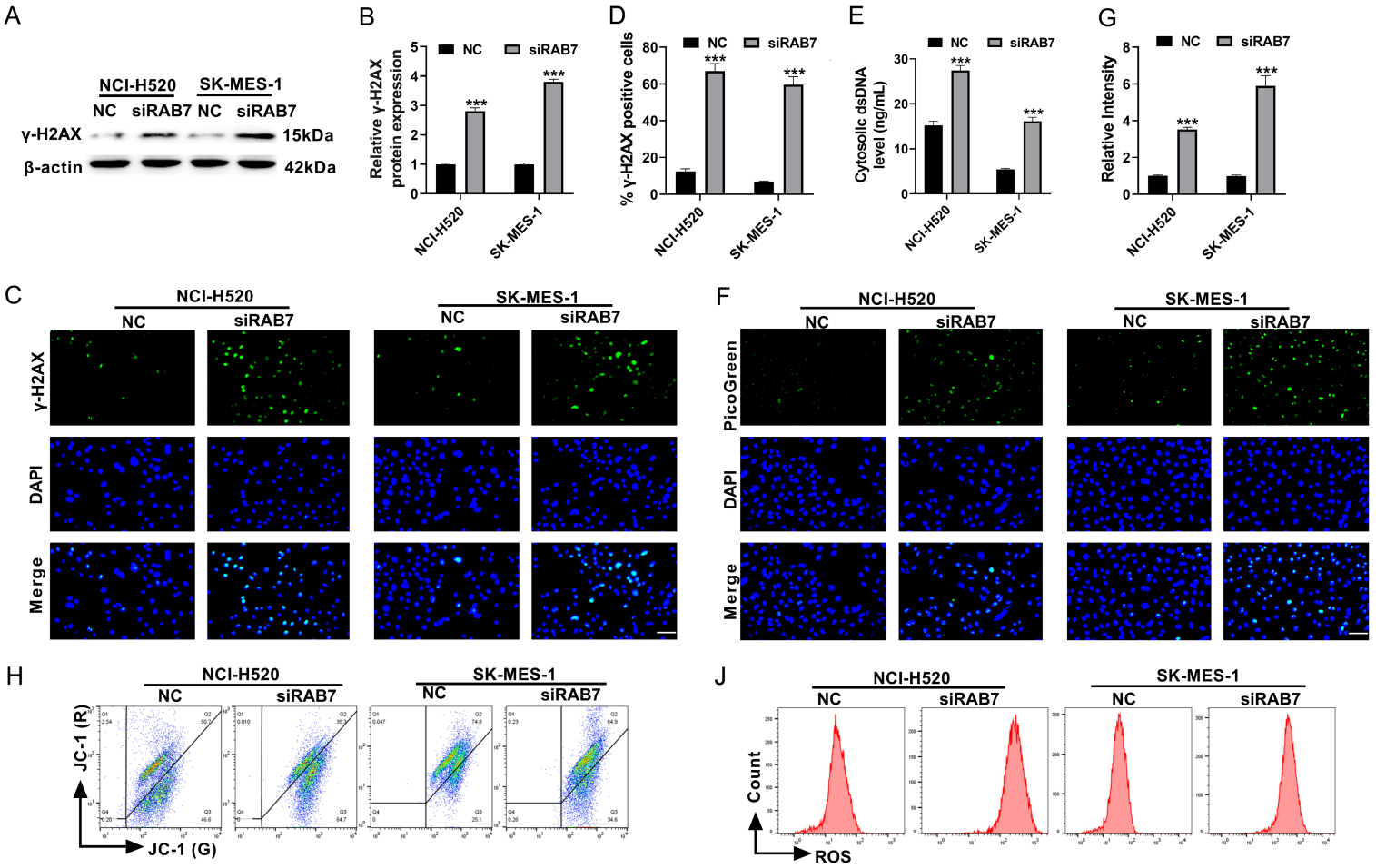

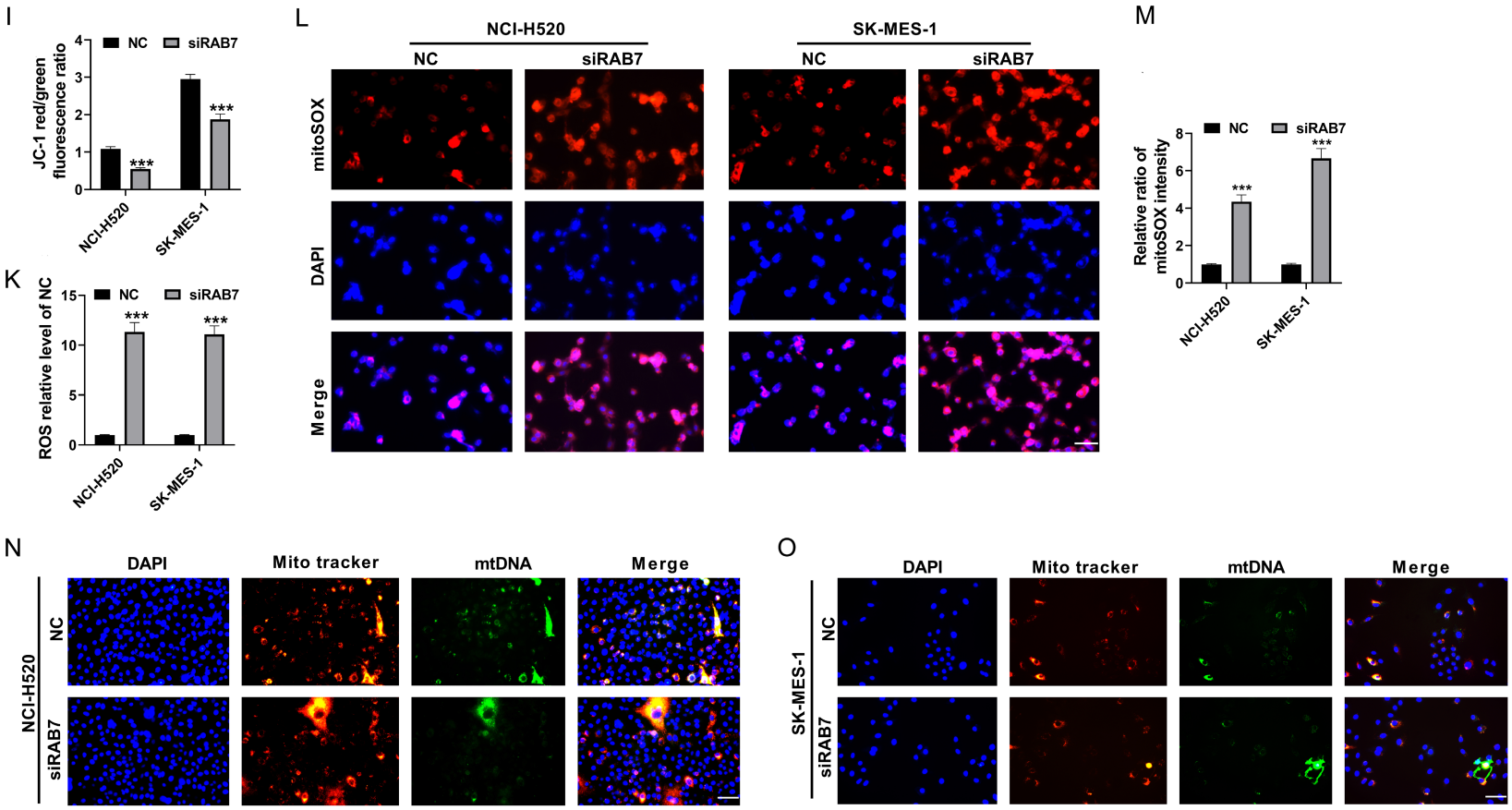

Figure 2. Knockdown of RAB7 promoted the accumulation of cytoplasmic dsDNA. A, B. Western blot analyzed DNA damage marker γ-H2AX protein expression. C, D. Immunofluorescence detected the formation of γ-H2AX (×40, 50 μm). E. Picogreen dsDNA quantitative fluorescence was used to evaluate cytoplasmic dsDNA. F, G. dsDNA expression was detected by immunofluorescence (×40, 50 μm). H, I. JC-1 fluorescent probe detected MMP levels. J, K. DFCH-DA detected intracellular ROS levels. L, M. MitoSOX Red measured mtROS levels (×40, 50 μm). N, O. DNA and mitochondria were double-labeled by immunofluorescence. Mitochondria were stained with MitoTracker (red), and dsDNA was stained with dsDNA antibody (green) (×40, 50 μm). ***$P < 0.001$ *vs* NC group. Notes: dsDNA, double-stranded DNA; γ-H2AX, phosphorylation of histone H2AX; MMP, mitochondrial membrane potential; ROS, reactive oxygen species; mtROS, mitochondrial reactive oxygen species.

accumulation. These results together indicated that knockdown of RAB7 induced mitochondrial dysfunction and oxidative stress, which in turn led to mtDNA leakage into the cytoplasm.

Knockdown of RAB7 promoted CD8⁺ T cell activity and enhanced the killing effect on lung cancer cells

Following the TIMER 2.0 database analysis, RAB7 expression was related to many immune cell infiltration, and the negative correlation with CD8⁺ T cells was the most significant (**Figure 3A**). In order to verify its function, CD8⁺ T cells were extracted and activated, then RAB7 knockdown LUSC cells were co-cultured with CD8⁺ T cells (**Figure 3B**). Knockdown of RAB7 promoted CD8⁺ T cell proliferation in the co-culture system (**Figure 3C**, **3D**). Knockdown of RAB7 accelerated CD8⁺ T cell recruitment into LUSC cells (**Figure 3E**), indicating that knockdown of RAB7 promoted CD8⁺ T cell penetration into tumor area. Knockdown of RAB7 enhanced CD8⁺ T cell toxicity to tumor cells (**Figure 3F**). Moreover, after RAB7 knockdown, the protein levels of effector molecules IFN-γ, GZMB and Perforin in co-cultured CD8⁺ T cells were raised, and exhaustion markers PD-1 and CD39 protein expressions were declined (**Figure 3G-I**). Further apoptosis experiments confirmed that apoptotic cell proportion in RAB7 knockdown cells after co-cultured were much higher than those of LUSC cells (**Figure 3J-L**), indicating that CD8⁺ T cells co-cultured with RAB7 knockdown tumor cells could more effectively induce tumor cell apoptosis. These results indicated that knockdown of RAB7 enhanced the killing effect on LUSC cells by enhancing CD8⁺ T cell activation and cytotoxicity and alleviating their depletion. In order to further verify the immune regulation function of RAB7 in antigen-specific system, we constructed UN-SCC679-OVA cells and co-cultured them with CD8⁺ T cells derived from OT-I mice. The experimental schematic diagram was shown in **Figure 3M**. Flow cytometry analysis showed that knockdown of RAB7 significantly increased the expression level of SIINFEKL-H-2Kb complex on the surface of UN-SCC679-OVA cells (**Figure 3N**), suggesting that RAB7 deficiency might enhance the immunogenicity of tumor cells by affecting antigen processing or MHC-I molecule delivery. Subsequently, we used different proportions of OT-I CD8⁺ T cells to co-culture with RAB7 knockdown UN-SCC679-OVA cells for 24 h. The optimal effector-target ratio was determined by gradient co-culture experiments as OT-I CD8⁺ T cells: tumor cells = 5:1 (**Figure 3O**). On this basis, ELISA detection showed that knockdown of RAB7 significantly increased the secretion levels of IFN-γ, GZMB and TNF-α in the culture supernatant (**Figure 3P-R**), and also promoted tumor cell apoptosis (**Figure 3S**). To confirm the antigen specificity of the killing effect, we treated tumor cells with αH-2Kb. The results showed that it blocked the apoptosis of tumor cells enhanced by RAB7 knockdown (**Figure 3T**), demonstrating that this effect depended on the specific recognition of the antigen peptide-MHC-I complex. In summary, knockdown of RAB7 increased the level of MHC-I in tumor cells, which in turn significantly enhances the activation and targeted killing ability of CD8⁺ T cells.

Knockdown of RAB7 activated the STING/IRF1 signaling axis

Cytoplasmic dsDNA accumulation is a key initial step in activating the STING signaling pathway. The STING/IRF1 signaling axis is concerned with regulating immune responses in tumor cells [17]. In RAB7 knockdown LUSC cells, p-STING and IRF1 and their downstream chemokines CCL5 and CXCL10 proteins were significantly increased (**Figure 4A-C**), suggesting that knockdown of RAB7 might activate the STING/IRF1 signaling axis. Moreover, Western blot and ELISA results showed that the level of cGAS of RAB7 knockdown cells were much higher than those of LUSC cells (**Figure 4D-F**), suggesting that the cGAS-STING/IRF1 signaling axis was activated. To further validate the function of this signal axis, siSTING and siNC were transfected into LUSC cells in this study, siSTING successfully knocked down STING (**Figure 4G**, **4H**). Subsequently, a double knockdown experiment of RAB7 and STING was performed in NCI-H520 cells. Simultaneous knockdown of STING inhibited the STING/IRF1/CCL5/CXCL10 signaling pathway (**Figure 4I**, **4J**). In summary, knockdown of RAB7 activated the STING/IRF1 signaling axis.

Knockdown of RAB7 activated STING/IRF1 pathway to inhibit lung cancer cell malignant phenotype and promote CD8⁺ T cell activation

In addition, compared with knockdown of RAB7 alone, the cell viability (**Figure 5A**), colony num-

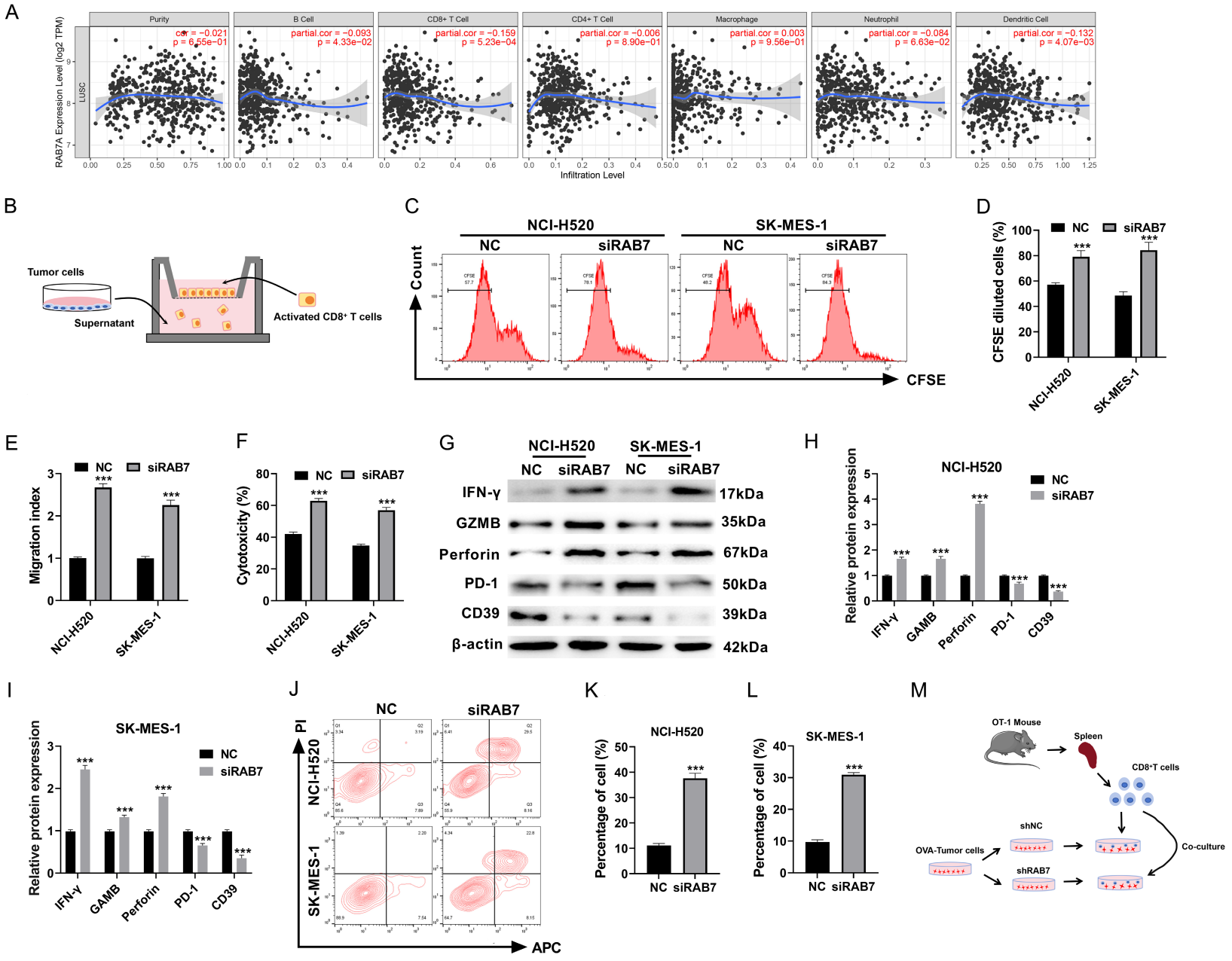
A
Purity
B Cell
CD8+ T Cell
CD4+ T Cell
Macrophage
Neutrophil
Dendritic Cell
RAB7A Expression Level (log2 TPM)
LUSC
Infiltration Level
B
Tumor cells
Supernatant
Activated CD8+ T cells
C
NCI-H520
SK-MES-1
NC
siRAB7
Count
CFSE
D
CFSE diluted cells (%)
E
Migration index
F
Cytotoxicity (%)
G
IFN-γ
GZMB
Perforin
PD-1
CD39
β-actin
17kDa
35kDa
67kDa
50kDa
39kDa
42kDa
H
Relative protein expression
I
J
PI
APC
K
Percentage of cell (%)
L
M
OT-1 Mouse
Spleen
CD8+T cells
shNC
shRAB7
OVA-Tumor cells
Co-culture

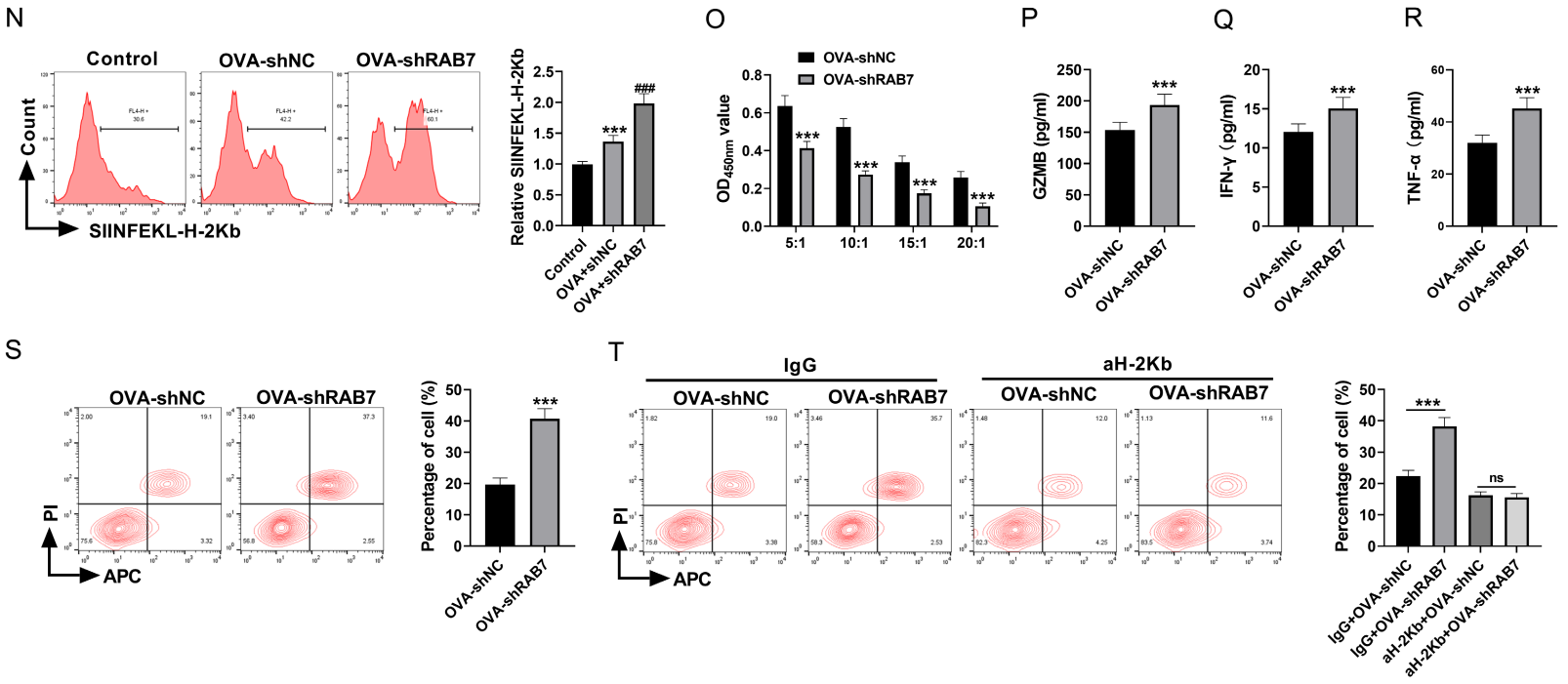

Figure 3. Knockdown of RAB7 promoted CD8$^+$ T cell activity and enhanced killing effect on lung cancer cells. A. TIMER 2.0 database analyzed the correlation between RAB7 and various immune cells. B. The schematic diagram of co-culture of human CD8$^+$ T cells and LUSC cells. C, D. CFSE assay detected CD8$^+$ T cell proliferation. E. Transwell assay counted CD8$^+$ T cells penetrating the membrane. F. LDH kit detected CD8$^+$ T cell cytotoxicity. G-I. Western blot detected CD8$^+$ T cell-related protein (IFN-γ, GZMB, Perforin, PD-1 and CD39) expressions. J-L. Flow cytometry detected LUSC cell apoptosis in the co-culture system. M. The experimental flow chart of isolation, activation and co-culture with UN-SCC679-OVA cells of CD8$^+$ T cells derived from OT-I mice. N. The expression level of SIINFEKL-H-2Kb complex on the surface of UN-SCC679-OVA cells was detected by flow cytometry. O. CCK-8 assay was used to detect the killing efficiency of OT-I CD8$^+$ T cells against UN-SCC679-OVA cells at different effector-target ratios. P-R. The concentrations of IFN-γ, GZMB and TNF-α in the co-culture system of UN-SCC679-OVA cells and OT-I CD8$^+$ T cells were detected by ELISA. S. The apoptosis rate of tumor cells in the co-culture system of UN-SCC679-OVA cells and OT-I CD8$^+$ T cells was detected by flow cytometry. T. αH-2Kb or IgG was added to the co-culture system of UN-SCC679-OVA cells and OT-I CD8$^+$ T cells. The apoptosis rate of tumor cells was detected by flow cytometry. $^{***}P < 0.001$ *vs* NC group. Notes: CFSE, carboxyfluorescein succinimidyl ester; LDH, lactate dehydrogenase; IFN-γ, interferon-γ; GZMB, Granzyme B; PD-1, programmed cell death protein 1.

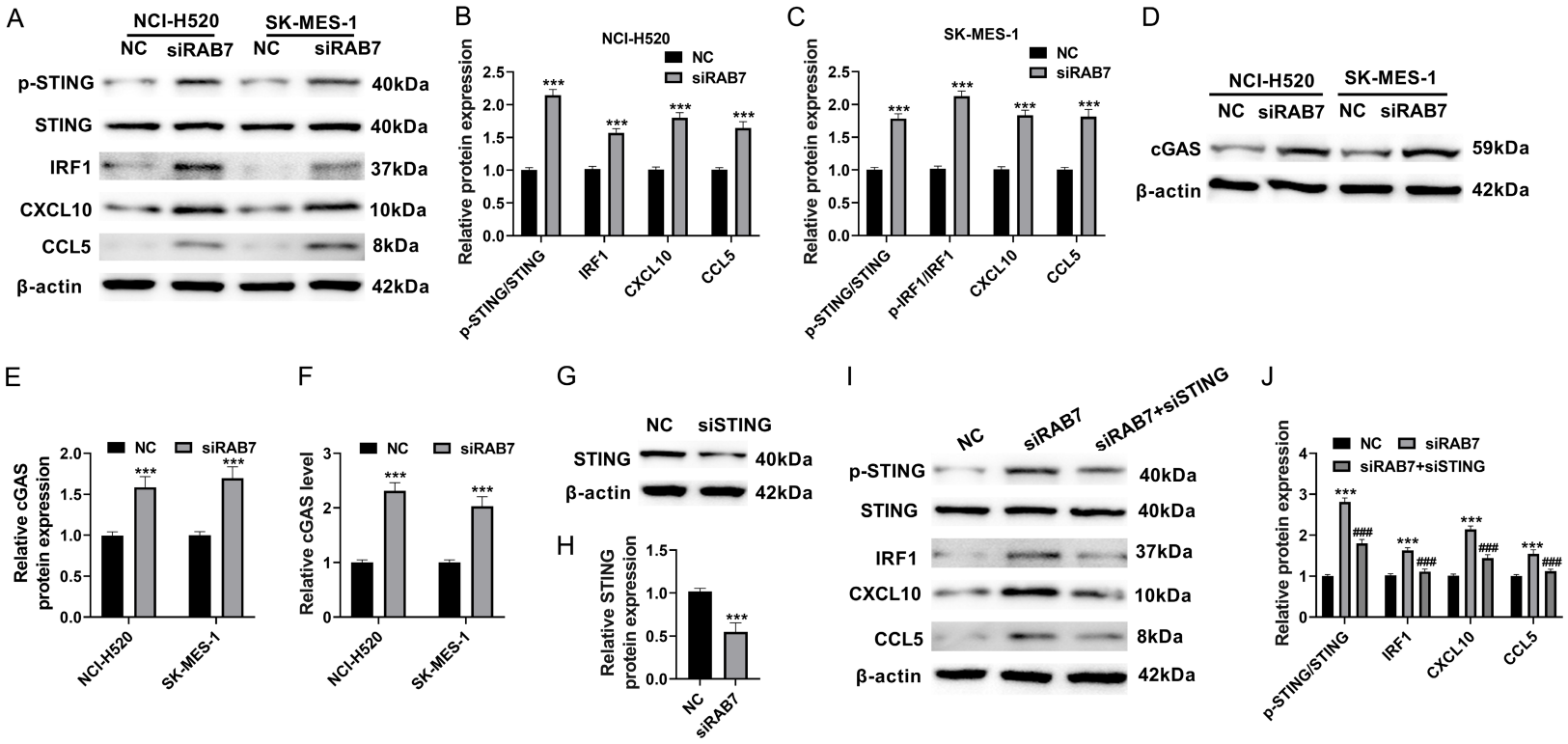

Figure 4. Knockdown of RAB7 activated the STING/IRF1 signaling axis. A-C. Western blot detected STING/IRF1 signal axis protein (p-STING, STING, IRF1, CCL5 and CXCL10) expression. D, E. The level of cGAS protein was detected by Western blot. F. The level of cGAS was detected by ELISA. G, H. siSTING and siNC were transfected into LUSC cells, and STING knockdown efficiencies were analyzed using Western blot. I, J. RAB7 and STING in NCI-H520 cells were knocked down at the same time, and the expression of STING/IRF1 signal axis proteins (p-STING, STING, IRF1, CCL5 and CXCL10) was analyzed using Western blot. ***$P < 0.001$ *vs* NC group; ###$P < 0.001$ *vs* siRAB7 group. Notes: STING, stimulator of interferon gene; IRF1, interferon regulatory factor 1; CCL5, C-C motif chemokine ligand 5; CXCL10, C-X-C motif chemokine ligand 10; cGAS, cyclic GMP-AMP synthase; ELISA, enzyme-linked immunosorbent assay.

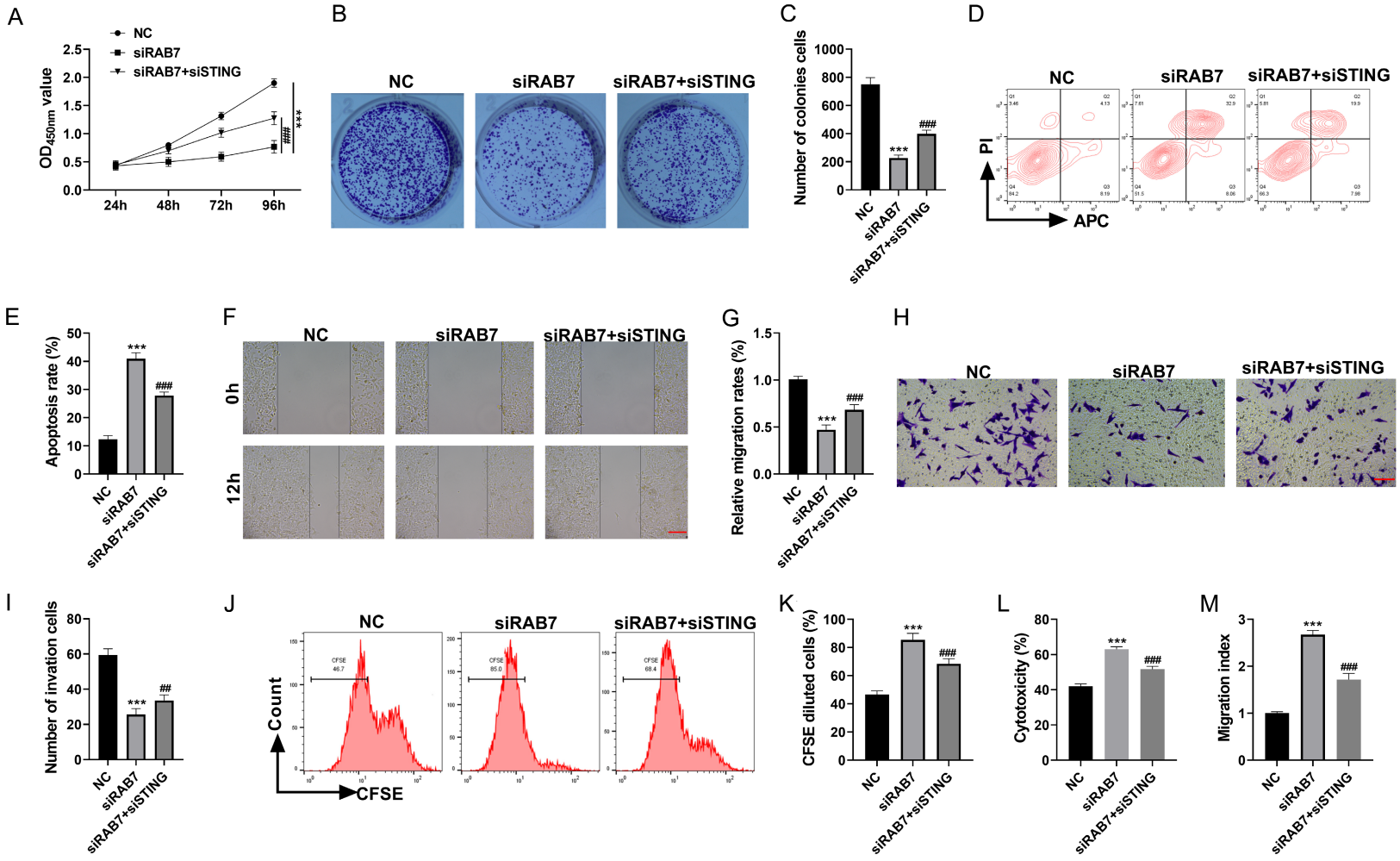
A
NC
siRAB7
siRAB7+siSTING
OD450nm value
24h
48h
72h
96h
***
###
B
NC
siRAB7
siRAB7+siSTING
C
Number of colonies cells
***
###
D
NC
siRAB7
siRAB7+siSTING
PI
APC
E
Apoptosis rate (%)
***
###
F
NC
siRAB7
siRAB7+siSTING
0h
12h
G
Relative migration rates (%)
***
###
H
NC
siRAB7
siRAB7+siSTING
I
Number of invation cells
***
##
J
NC
siRAB7
siRAB7+siSTING
Count
CFSE
K
CFSE diluted cells (%)
***
###
L
Cytotoxicity (%)
***
###
M
Migration index
***
###

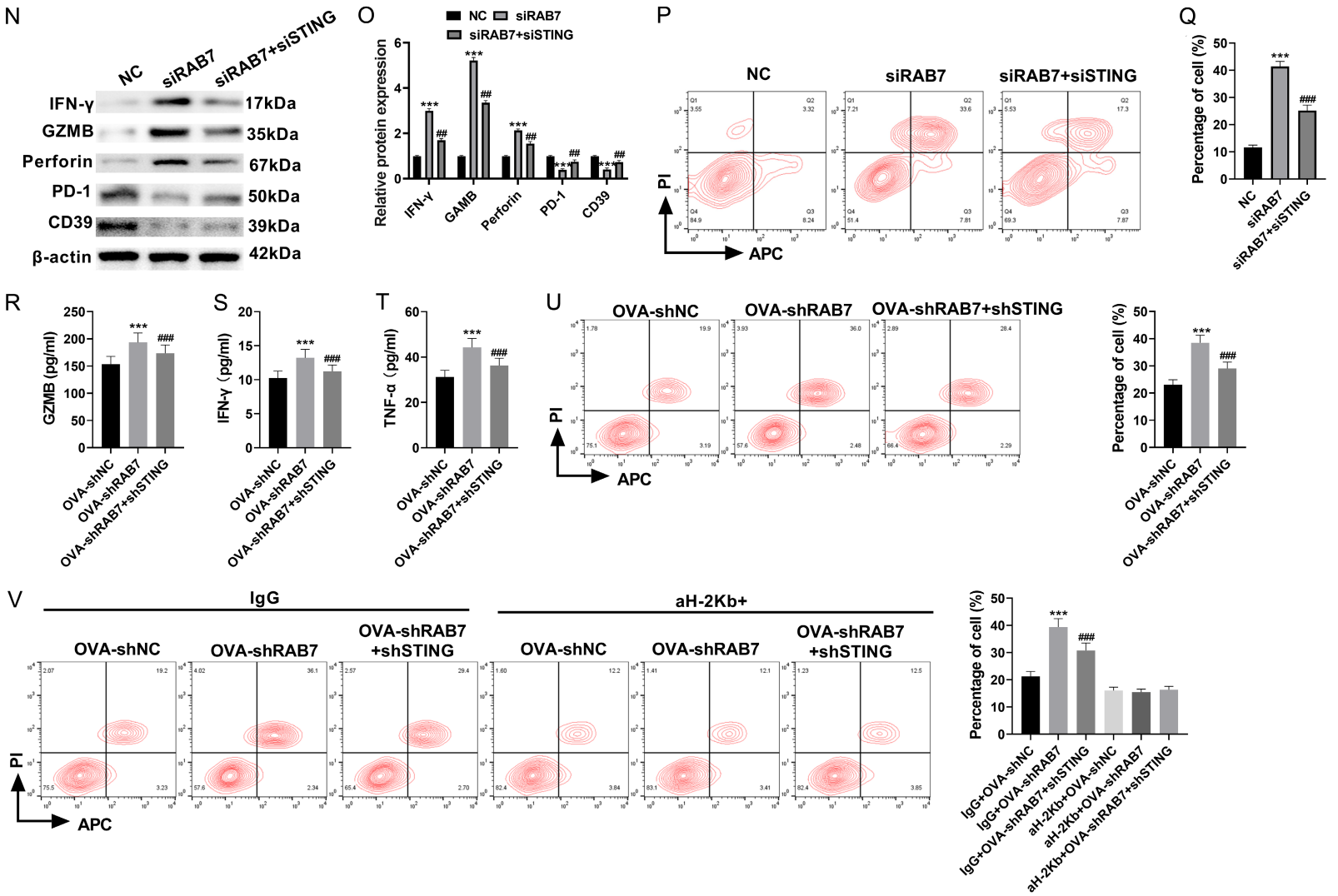

Figure 5. Knockdown of RAB7 activated STING/IRF1 pathway to inhibit the malignant phenotype of lung cancer cells and promote CD8⁺ T cell activity. A. CCK-8 assays detected NCI-H520 cell viability. B, C. NCI-H520 cell proliferation was observed using plate colony formation assay. D, E. Flow cytometry detected NCI-H520 cell apoptosis. F, G. Cell scratch assays detected NCI-H520 cell migration (×10, 200 μm). H, I. Transwell assays detected NCI-H520 cell invasion (×20, 100 μm). J, K. CFSE assay detected CD8⁺ T cell proliferation in the co-culture system. L. Transwell assay counted CD8⁺ T cells penetrating membrane. M. LDH kit detected CD8⁺ T cell cytotoxicity. N, O. Western blot detected CD8⁺ T cell-related protein (IFN-γ, GZMB, Perforin, PD-1 and CD39) expressions. P, Q. Flow cytometry detected NCI-H520

cell apoptosis in co-culture system. R-T. The concentrations of IFN-γ, GZMB and TNF-α in the co-culture system of UN-SCC679-OVA cells and OT-I CD8$^+$ T cells were detected by ELISA. U. The apoptosis rate of tumor cells in the co-culture system of UN-SCC679-OVA cells and OT-I CD8$^+$ T cells was detected by flow cytometry. V. αH-2Kb or IgG was added to the co-culture system of UN-SCC679-OVA cells and OT-I CD8$^+$ T cells. The apoptosis rate of tumor cells was detected by flow cytometry. ***P < 0.001 *vs* NC group; ##P < 0.01, ###P < 0.001 *vs* siRAB7 group.

ber (**Figure 5B**, **5C**), migration rate (**Figure 5F**, **5G**) and number of invasive cells (**Figure 5H**, **5I**) of NCI-H520 cells with simultaneous STING knockdown were much higher than those of NC group, with only a few apoptotic cells (**Figure 5D**, **5E**). At the same time, knockdown of STING suppressed CD8$^+$ T cell proliferation (**Figure 5J**, **5K**), inhibited CD8$^+$ T cell recruitment into tumor cells (**Figure 5L**), weakened CD8$^+$ T cell cytotoxicity (**Figure 5M**), reduced the expression of IFN-γ, GZMB and Perforin proteins, and increased PD-1 and CD39 proteins (**Figure 5N**, **5O**). In addition, knockdown of STING also reduced NCI-H520 cell apoptosis rates in the co-culture system (**Figure 5P**, **5Q**). This indicated that knockdown of STING could partially weaken CD8$^+$ T cell activation and killing effect. These results fully demonstrate that RAB7 knockdown suppresses LUSC cell malignant phenotype and the promotion of CD8$^+$ T cell activation mainly depends on STING/IRF1 axis activation. Subsequently, in the co-culture system of UN-SCC679-OVA cells and OT-I CD8$^+$ T cells, compared with RAB7 knockdown alone, simultaneous knockdown of STING significantly reduced the levels of GZMB, IFN-γ and TNF-α (**Figure 5R-T**) and decreased tumor cell apoptosis rate (**Figure 5U**). And αH-2Kb also blocked the killing of OT-I CD8$^+$ T cells on all groups of tumor cells (**Figure 5V**). More importantly, under the background of antibody blocking, there was no significant difference in the apoptosis rate between the groups, further excluding the interference of non-specific cytotoxic effects. This proved that the cytotoxicity in this model depended on the recognition of the antigen peptide-MHC-I complex.

Knockdown of RAB7 synergized with PD-1 antibody to suppress lung tumor growth

In the subcutaneously transplanted UN-SCC-679 cell model of C57BL/6 mice, RAB7 was knocked down by shRNA, and RAB7 was successfully knocked down (**Figure 6A**, **6B**). Knockdown of RAB7 or anti-PD-1 treatment reduced the volume and weight of subcutaneous tumors by about 50%, and tumor growth was inhibited, and the combination of the two treatments could further enhance the anti-tumor effect, it was manifested by reduced cancer volume and tumor weight (**Figure 6C-E**). In addition, the number of Ki67 positive cells in tumor tissues treated with knockdown of RAB7 or anti-PD-1 treatment was much lower than that in the NC group (**Figure 6F**, **6G**), and the number of TUNEL positive cells was much higher than that in the NC group (**Figure 6H**, **6I**), and the effect of combined treatment was the most significant. In summary, knockdown of RAB7 effectively enhanced anti-PD-1 anti-tumor efficacy, synergistically suppressed lung cancer growth and promote its apoptosis.

Knockdown of RAB7 synergized with PD-1 antibody to activate STING/IRF1/CCL5/CXCL10 pathway and enhance CD8$^+$ T cell activity

In the tumor-bearing mouse model, knockdown of RAB7 or anti-PD-1 treatment significantly activated the STING/IRF1/CCL5/CXCL10 signaling pathway in tumor tissues, and the combined activation effect of the two was the most significant (**Figure 7A**, **7B**). Knockdown of RAB7 reduced RAB7 fluorescence intensity, and raised CD8 fluorescence intensity (**Figure 7C-E**). Flow cytometry analysis further showed that after knockdown of RAB7 or anti-PD-1 intervention, tumor tissues showed many CD8$^+$ T cell infiltrations (**Figure 7F**, **7G**), and IFN-γ, GZMB and Perforin protein increased, while PD-1 and CD39 protein decreased (**Figure 7H**, **7I**), and the combination of the two enhanced CD8$^+$ T cell activity most significantly. Knockdown of RAB7 enhanced CD8$^+$ T cell infiltration and activity by activating STING/IRF1/CCL5/CXCL10 signaling axis, thereby exerting synergistic anti-cancer effects with anti-PD-1.

Discussion

This study first established the carcinogenic role of RAB7 in lung cancer. We confirmed that RAB7 was high expressed in a variety of LUSC cells (NCI-H520, SK-MES-1, HCC827 and NCI-

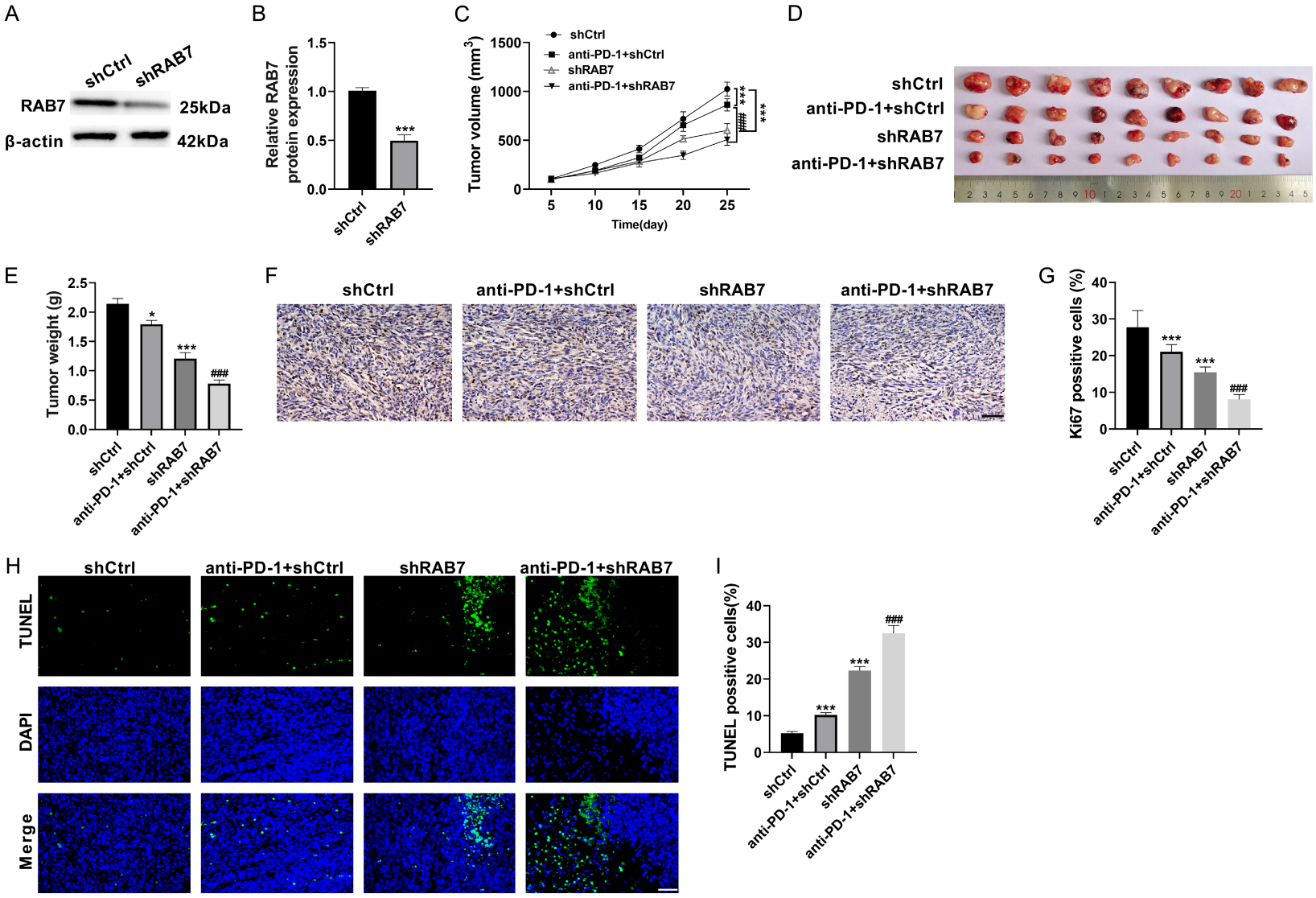

Figure 6. RAB7 knockdown synergized with PD-1 antibody to suppress lung tumor growth. A, B. The knockdown efficiency of RAB7 in subcutaneous tumor tissues was detected by Western blot. C-E. Morphological image, cancer volume and weight of tumors in mice. F, G. Ki67 immunohistochemical representative images and histograms of tumors (×40, 50 μm). H, I. TUNEL staining of tumors represented images and histograms (×40, 50 μm). *$P < 0.05$, ***$P < 0.001$ *vs* shCtrl group; ###$P < 0.001$ *vs* shCtrl+anti-PD-1 group.

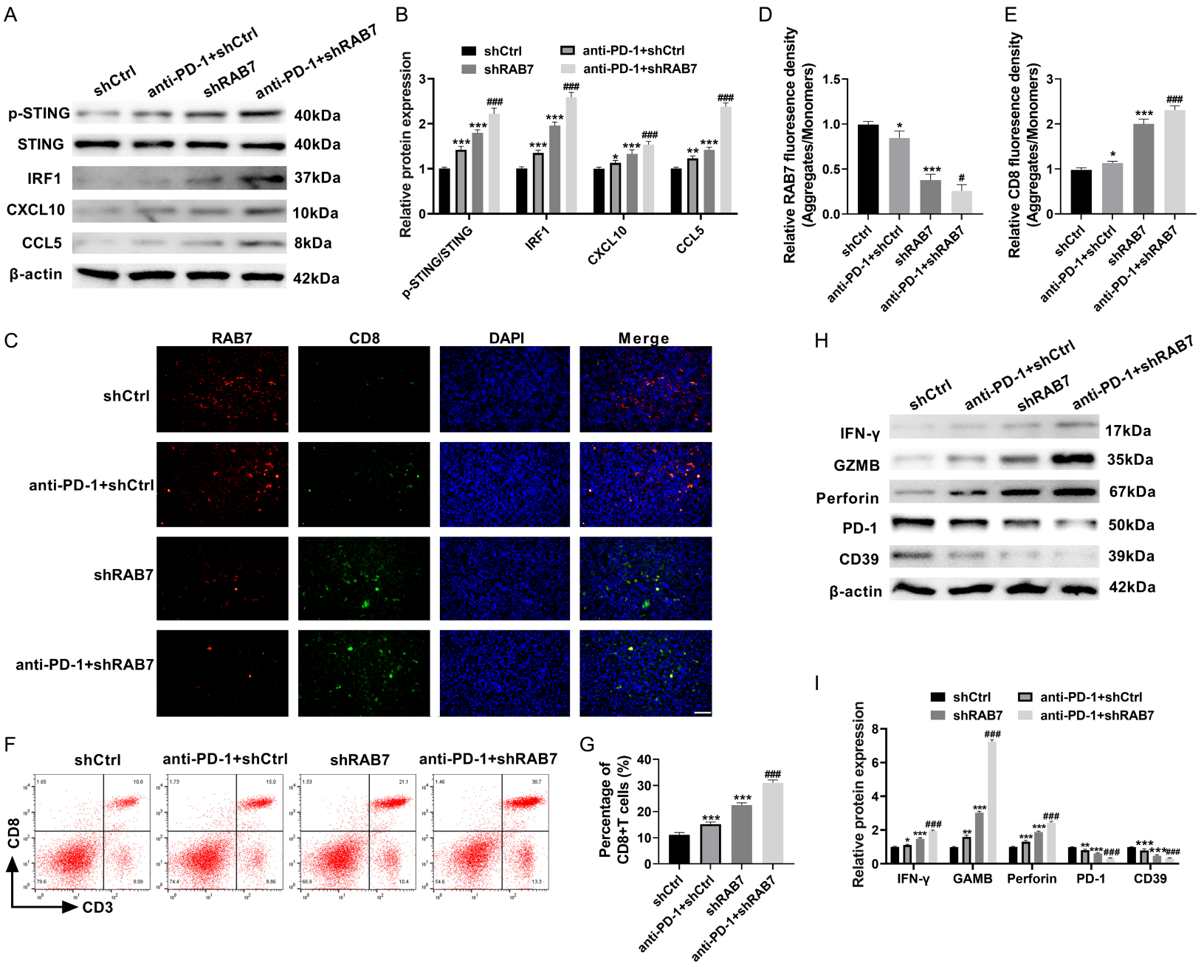
A
shCtrl
anti-PD-1+shCtrl
shRAB7
anti-PD-1+shRAB7
p-STING
STING
IRF1
CXCL10
CCL5
β-actin
40kDa
40kDa
37kDa
10kDa
8kDa
42kDa
B
shCtrl
shRAB7
anti-PD-1+shCtrl
anti-PD-1+shRAB7
Relative protein expression
p-STING/STING
IRF1
CXCL10
CCL5
D
Relative RAB7 fluoresence density (Aggregates/Monomers)
E
Relative CD8 fluoresence density (Aggregates/Monomers)
C
RAB7
CD8
DAPI
Merge
shCtrl
anti-PD-1+shCtrl
shRAB7
anti-PD-1+shRAB7
H
IFN-γ
GZMB
Perforin
PD-1
CD39
β-actin
17kDa
35kDa
67kDa
50kDa
39kDa
42kDa
F
CD8
CD3
G
Percentage of CD8+T cells (%)
I
Relative protein expression
IFN-γ
GAMB
Perforin
PD-1
CD39

Figure 7. Knockdown of RAB7 synergized with PD-1 antibody to activate STING/IRF1/CCL5/CXCL10 pathway and enhance CD8$^+$ T cell activity. A, B. Western blot detected STING/IRF1 signal axis proteins (p-STING, STING, IRF1, CCL5 and CXCL10). C-E. CD8 immunofluorescence representative images and histograms of tumors (×40, 50 μm). F, G. Tumor-infiltrating CD8$^+$ T cell proportion was analyzed by flow cytometry. H, I. Western blot detected CD8$^+$ T cell-related protein (IFN-γ, GZMB, Perforin, PD-1 and CD39) expressions. *P < 0.05, **P < 0.01, ***P < 0.001 *vs* shCtrl group; #P < 0.05, ###P < 0.001 *vs* shCtrl+anti-PD-1 group.

H226), RAB7 may have a vital impact on lung cancer development, which is consistent with some recent studies on RAB7 promoting tumor progression [23, 24]. Subsequently, RAB7 knockdown plasmids were transfected into NCI-H520 and SK-MES-1 cells. After RAB7 knockdown, LUSC cell proliferation, movement and invasion were significantly decreased, and the apoptosis rate was increased, indicating that knockdown of RAB7 can inhibit the malignant phenotype of lung cancer. This suggests that RAB7 is vital for lung cancer malignant biological behavior.

More importantly, we found a new function of RAB7 in regulating tumor immune microenvironment. TIMER2.0 database analysis showed that RAB7 was negatively correlated with CD8$^+$ T cell infiltration, which provided initial clues for our subsequent exploration of immune function. CD8$^+$ T cells are vital for antitumor immunity. Effector CD8$^+$ T cells can exert their cytotoxic effects by releasing effector molecules such as TNF-α, INF-γ, GZMB and Perforin [29]. Through *in vitro* co-culture experiments, RAB7 knockdown directly enhanced CD8$^+$ T cell proliferation, migration, and cytotoxicity, while increasing the expression of its effector molecules (IFN-γ, GZMB, Perforin) and reducing depletion marker levels (PD-1 and CD39). Crucially, to distinguish tumor antigen-specific immunity from non-specific allogeneic responses, OT-I CD8$^+$ T cells and UN-SCC679-OVA cells were co-cultured. In this model, RAB7 knockdown significantly enhanced the surface expression of the SIINFEKL-H-2Kb complex, directly linking RAB7 knockdown with improved antigen presentation. Thus, we observed that the activation of CD8$^+$ T cells, the secretion of cytokines, and the killing effect of target cells were significantly enhanced, and these phenomena were dependent on the recognition of MHC-I, which was confirmed by the blocking antibody αH-2Kb. This discovery extends the function of RAB7 from the traditional autonomous survival of tumor cells to a new dimension of regulating adaptive immune response.

DNA, as an immune stimulating factor, is recognized by pattern recognition receptors to initiate innate immune responses and further induce the formation of adaptive immunity. This dual immune mechanism works together to provide an effective defense barrier for the body, and is concerned with regulating various pathological processes including microbial infection, autoimmune, inflammation, and organ degradation [30]. The functional integrity of autophagy is essential for maintaining intracellular homeostasis. LC3 and p62 are biomarkers of autophagy. Among them, p62 is the first identified selective autophagy receptor protein, which can drive ubiquitination-dependent autophagy degradation [31]. cGAS-STING axis is an important pathway in identifying cytoplasmic DNA and an important signaling cascade in innate immunity [32]. The cytoplasmic dsDNA also activates the cGAS-STING pathway, allowing STING to respond to STING's own degradation and attenuation by phosphorylating p62 [33]. Therefore, in the negative feedback loop activated by the STING pathway, autophagy is vital for ensuring that the STING signal can be transmitted instantaneously, effectively avoiding the excessive activation of the pathway, thereby maintaining the physiological homeostasis of the human body [34]. Our data showed that knockdown of RAB7 significantly increased p62 and LC3B-II/I protein levels, blocked autophagy flux, resulting in a large accumulation of autophagosomes and a significant reduction in autophagic lysosomes. Crucially, knockdown of RAB7 led to loss of MMP and increased ROS levels, inducing mitochondrial dysfunction. Mitochondria with impaired function cannot be removed in time, resulting in mtDNA leakage to the cytoplasm. More importantly, we observed a significant increase in cytoplasmic dsDNA and a notable increase in γ-H2AX content, as well as a significant increase in cGAS levels. The destruction of autophagic flux makes the stress signals of endogenous genomes (such as damaged mitochondrial DNA or nuclear DNA fragments) unable to be cleared in time and thus perceived

by cGAS in the cytoplasm. This finding echoes previous studies that autophagy-related proteins can negatively regulate the cGAS-STING pathway, forming a feedback loop [35-37]. Our study highlights the key role of RAB7 in this process.

Subsequently, we confirmed that knockdown of RAB7 significantly activated the STING/IRF1/CCL5/CXCL10 signaling. The innate immune response mediated by the this pathway is vital for inhibiting tumor development through cell-autonomous and non-cell-autonomous signal transduction, thereby forming immune cell-mediated tumor suppression [38]. Li *et al.* found that overexpression of IRF1 can up-regulate CXCL10, thereby promoting $CD8^+$ T cell accumulation to reduce tumor growth [39]. The STING/IRF1 signaling axis regulates cancer cell immune responses triggered by fractionated irradiation [17]. It has been reported that Brazilin can significantly activate the STING/IRF3/CCL5/CXCL10 signaling pathway, and inhibit the proliferation of NSCLC [40]. Tan *et al.* also found that tetrandrine can increase cytoplasmic dsDNA, thereby activating the STING/TBK1/IRF3 signaling pathway, thereby promoting $CD8^+$ T lymphocyte infiltration and enhancing the efficacy of NSCLC anti-PD-1 immunotherapy [41]. In this study, simultaneous knockdown of RAB7 and STING significantly promoted NCI-H520 cell malignant biological behavior, and significantly weakened the activation, toxic effects and tumor clearance of $CD8^+$ T cells. These results fully demonstrate that RAB7 knockdown inhibits lung cancer cell malignant phenotype and the promotion of $CD8^+$ T cell activation mainly depends on the activation of STING/IRF1/CCL5/CXCL10 signaling pathway.

An intriguing observation in our study is that STING knockdown partially reduced the levels of γ-H2AX and cytoplasmic dsDNA induced by RAB7 inhibition. Since STING is a downstream adaptor of DNA sensing rather than a direct regulator of DNA damage or release, this effect likely reflects an indirect, feedback-dependent stabilization of the immunogenic state. Activated STING can promote cellular senescence, modulate mitochondrial ROS production, and engage crosstalk with the DNA damage response machinery. Thus, loss of STING signaling may allow cells to recover from the initial genomic stress triggered by RAB7 inhibition, leading to diminished DNA damage markers and reduced dsDNA accumulation. This interpretation aligns with emerging evidence that STING signaling not only transmits innate immune signals but also actively shapes the cellular stress landscape [30, 42].

Our *in vivo* experiments found that knockdown of RAB7 alone has shown anti-tumor effects, and when combined with PD-1 antibody, it has a significant synergistic effect, which greatly inhibits tumor growth, accompanied by a decrease in $Ki67^+$ tumor cells and an increase in apoptosis. The analysis of intratumoral tissues further confirmed that the STING/IRF1 pathway was strongly activated in the combined treatment group, and the infiltration and functional status of $CD8^+$ T cells also reached a better level. This finding has important clinical significance because it provides a novel joint strategy to overcome the resistance of PD-1 inhibitors.

This study systematically revealed the key role and molecular mechanism of targeted knockdown of RAB7 in enhancing the efficacy of anti-PD-1 in the treatment of lung cancer. Our results together show that inhibition of RAB7 can not only directly inhibit the malignant behavior of lung cancer cells, but also lead to cytoplasmic dsDNA accumulation by destroying autophagy flux, activate the STING/IRF1/CCL5/CXCL10 signaling axis, and ultimately reshape the tumor immune microenvironment, enhance the activation and killing function of $CD8^+$ T cells, thus producing a strong synergistic antitumor effect with PD-1 antibody.

Of course, this study also has some limitations. First of all, the research mainly depends on the established tumor cell lines. In the future, it needs to be verified in the patient-derived organoids or primary cell models to be closer to the clinical reality. Secondly, the specific role of RAB7 in different cell types in the TME has not been clarified, and the use of gene knockout animal models will be able to more accurately analyze its cell-specific functions. Third, knockdown of STING partially attenuates RAB7 knockdown-induced DNA damage signals. Given that STING is a downstream adaptor protein, this phenomenon suggests that its function may exceed classical signal transduction, or indirectly affect genomic stability by non-specific pathways such as increasing endoplasmic reticulum stress and interfering with cell cycle

[42, 43]. In the future, more sophisticated models are needed to analyze this complex interaction. Finally, although we have confirmed that mitochondrial DNA leakage is an important source of dsDNA, the role of other potential sources (such as nuclear DNA leakage) and whether other DNA receptors other than cGAS are involved remain to be further explored.

Conclusion

In summary, knockdown of RAB7 activates the STING/IRF1/CCL5/CXCL10 signaling pathway by blocking autophagy flux and accumulating cytoplasmic dsDNA, thereby recruiting and activating $CD8^+$ T cells and enhancing the efficacy of anti-PD-1 immunotherapy for lung cancer. Therefore, RAB7 is expected to provide a new direction for molecular targeted therapy of lung cancer, and provide a solid theoretical basis and prospect for clinical development of combined therapy targeting RAB7 and aiming at reversing immune resistance. However, considering the limitations of existing evidence, further large-sample, multi-center, high-quality randomized controlled trials should be carried out in the future to further verify the efficacy and safety of knocking down RAB7 combined with PD-1 antibody in the treatment of lung cancer.

Acknowledgements

This work is supported by: (1) Henan Province Science and Technology Research Project (232102311140); (2) Henan Province Health Commission Science and Technology Innovation Talent Project (JQRC2025005).

Disclosure of conflict of interest

None.

Abbreviations

PD-1, Programmed cell death protein 1; NSCLC, non-small cell lung cancer; PD-1, programmed cell death ligand 1; TILs, tumor-infiltrating lymphocytes; TEM, transmission electron microscope; TME, tumor microenvironment; dsDNA, double-stranded DNA; cGAS, cyclic GMP-AMP synthase; STING, stimulator of interferon gene; IRF, interferon regulatory factor; IFN, interferon; CCL5, C-C motif chemokine ligand 5; CXCL, C-X-C motif chemokine ligand; RAB7, RAS-associated binding protein 7; GTPase, small guanosine triphosphatase; LUSC, lung squamous cell carcinoma; FBS, fetal bovine serum; PBMCs, peripheral blood mononuclear cells; IL, interleukin; CFSE, carboxyfluorescein succinimidyl ester; LDH, Lactate dehydrogenase; LAMP1, lysosomal-associated membrane protein 1; LC3B, microtubule-light chain 3 Beta; GZMB, Granzyme B; γ-H2AX, phosphorylation of histone H2AX.

Address correspondence to: Huaimin Liu, Department of Integrated Traditional Chinese and Western Medicine, The Affiliated Cancer Hospital of Zhengzhou University and Henan Cancer Hospital, No. 127 Dongming Road, Jinshui District, Zhengzhou 450008, Henan, China. E-mail: LiuHuaimin1128@hotmail.com

References

[1] Bray F, Laversanne M, Sung H, Ferlay J, Siegel RL, Soerjomataram I and Jemal A. Global cancer statistics 2022: GLOBOCAN estimates of incidence and mortality worldwide for 36 cancers in 185 countries. CA Cancer J Clin 2024; 74: 229-263.

[2] Ma Z, Lv J, Zhu M, Yu C, Ma H, Jin G, Guo Y, Bian Z, Yang L, Chen Y, Chen Z, Hu Z, Li L and Shen H. Lung cancer risk score for ever and never smokers in China. Cancer Commun (Lond) 2023; 43: 877-895.

[3] Li C, Lei S, Ding L, Xu Y, Wu X, Wang H, Zhang Z, Gao T, Zhang Y and Li L. Global burden and trends of lung cancer incidence and mortality. Chin Med J (Engl) 2023; 136: 1583-1590.

[4] Miller KD, Nogueira L, Devasia T, Mariotto AB, Yabroff KR, Jemal A, Kramer J and Siegel RL. Cancer treatment and survivorship statistics, 2022. CA Cancer J Clin 2022; 72: 409-436.

[5] Wang M, Herbst RS and Boshoff C. Toward personalized treatment approaches for non-small-cell lung cancer. Nat Med 2021; 27: 1345-1356.

[6] Reck M, Remon J and Hellmann MD. First-line immunotherapy for non-small-cell lung cancer. J Clin Oncol 2022; 40: 586-597.

[7] Insa A, Martín-Martorell P, Di Liello R, Fasano M, Martini G, Napolitano S, Vicidomini G, Cappabianca S, Franco R, Morgillo F and Della Corte CM. Which treatment after first line therapy in NSCLC patients without genetic alterations in the era of immunotherapy? Crit Rev Oncol Hematol 2022; 169: 103538.

[8] Zhou X, Yao Z, Bai H, Duan J, Wang Z, Wang X, Zhang X, Xu J, Fei K, Zhang Z, Tan F, Xue Q, Gao S, Gao Y, Wang J and He J. Treatment-related

adverse events of PD-1 and PD-L1 inhibitor-based combination therapies in clinical trials: a systematic review and meta-analysis. Lancet Oncol 2021; 22: 1265-1274.
[9] Sas Z, Cendrowicz E, Weinhäuser I and Rygiel TP. Tumor microenvironment of hepatocellular carcinoma: challenges and opportunities for new treatment options. Int J Mol Sci 2022; 23: 3778.
[10] Paijens ST, Vledder A, de Bruyn M and Nijman HW. Tumor-infiltrating lymphocytes in the immunotherapy era. Cell Mol Immunol 2021; 18: 842-859.
[11] Miller BC, Sen DR, Al Abosy R, Bi K, Virkud YV, LaFleur MW, Yates KB, Lako A, Felt K, Naik GS, Manos M, Gjini E, Kuchroo JR, Ishizuka JJ, Collier JL, Griffin GK, Maleri S, Comstock DE, Weiss SA, Brown FD, Panda A, Zimmer MD, Manguso RT, Hodi FS, Rodig SJ, Sharpe AH and Haining WN. Subsets of exhausted CD8(+) T cells differentially mediate tumor control and respond to checkpoint blockade. Nat Immunol 2019; 20: 326-336.
[12] Zong Q, Zhang H, Liu F, Li J, Liu Q, Duan Z, Duan W, Ruan M, Zhang J, Liu Y, Zhou Q and Wang Q. Activation of the cGAS-STING pathway by viral dsDNA leading to M1 polarization of macrophages mediates antiviral activity against hepatitis B virus. Immunobiology 2024; 229: 152810.
[13] Wang J and Xing L. Therapeutic targeting of cGAS-STING pathway in lung cancer. Cell Biol Int 2025; 49: 129-138.
[14] Gayen S, Parui A, Arshad A, Roy N, Sarkar AN and Roy S. Decrypting the crosstalk mechanisms between cGAS-STING and TBK1 signaling pathways in cancer immunotherapy: a comprehensive review. Journal of Cancer Biomoleculars and Therapeutics 2025; 2: 89-104.
[15] Zhang Z, Zhou H, Ouyang X, Dong Y, Sarapultsev A, Luo S and Hu D. Multifaceted functions of STING in human health and disease: from molecular mechanism to targeted strategy. Signal Transduct Target Ther 2022; 7: 394.
[16] Duong E, Fessenden TB, Lutz E, Dinter T, Yim L, Blatt S, Bhutkar A, Wittrup KD and Spranger S. Type I interferon activates MHC class I-dressed CD11b(+) conventional dendritic cells to promote protective anti-tumor CD8(+) T cell immunity. Immunity 2022; 55: 308-323, e309.
[17] Du J, Kageyama SI, Yamashita R, Hirata H, Hakozaki Y, Okumura M, Motegi A, Hojo H, Nakamura M, Hirano Y, Sunakawa H, Minamide T, Kotani D, Tanaka K, Yano T, Kojima T, Ohashi A, Tsuchihara K and Akimoto T. Impacts of the STING-IFNAR1-STAT1-IRF1 pathway on the cellular immune reaction induced by fractionated irradiation. Cancer Sci 2022; 113: 1352-1361.
[18] Rangel M, Kong J, Bhatt V, Khayati K and Guo JY. Autophagy and tumorigenesis. FEBS J 2022; 289: 7177-7198.
[19] Wang H, Sun P, Yuan X, Xu Z, Jiang X, Xiao M, Yao X and Shi Y. Autophagy in tumor immune escape and immunotherapy. Mol Cancer 2025; 24: 85.
[20] Fischer P, Schmid M, Ohradanova-Repic A, Schneeweiss R, Hadatsch J, Grünert O, Benedum J, Röhrer A, Staudinger F, Schatzlmaier P, Bragato N, Barna S, Engl M, Kleinwächter A, Georg D, Widder J, Kerschbaum-Gruber S and Slade D. Molecular features of TNBC govern heterogeneity in the response to radiation and autophagy inhibition. Cell Death Dis 2025; 16: 540.
[21] Xu G, Shu Y, Jiang M, Zhang Y, Zhu J, Peng Y, Pu F, Ren J and Qu X. Intervention in the crosstalk between the cGAS-STING pathway and autophagy using an oligonucleotide-based bioorthogonal platform for amplifying immunotherapy. Nano Lett 2025; 25: 9834-9844.
[22] Guerra F and Bucci C. Role of the RAB7 protein in tumor progression and cisplatin Chemoresistance. Cancers (Basel) 2019; 11: 1096.
[23] Hu J, Ding X, Tian S, Chu Y, Liu Z, Li Y, Li X, Wang G, Wang L and Wang Z. TRIM39 deficiency inhibits tumor progression and autophagic flux in colorectal cancer via suppressing the activity of Rab7. Cell Death Dis 2021; 12: 391.
[24] Fernandez M, Wang R, Wang J, Wu S, Holder K, Nazarullah A, Aguiar RCT, Xu-Monette ZY, Young KH, Yan H and Xu Z. Targeting RAB7 in human B lymphoma by a small molecule inhibitor arrests tumor cell growth. Front Oncol 2025; 15: 1616519.
[25] Bai R, Rebelo A, Kleeff J and Sunami Y. Identification of prognostic lipid droplet-associated genes in pancreatic cancer patients via bioinformatics analysis. Lipids Health Dis 2021; 20: 58.
[26] Zhou C, Wei W, Ma J, Yang Y, Liang L, Zhang Y, Wang Z, Chen X, Huang L, Wang W and Wu S. Cancer-secreted exosomal miR-1468-5p promotes tumor immune escape via the immunosuppressive reprogramming of lymphatic vessels. Mol Ther 2021; 29: 1512-1528.
[27] Xing X, Yin SQ, Li XQ, Li H, Ma HT, Tulamaiti A, Xiao SY, Liu YT, Zhang H, Zhang Z, Huo YM, Yang XM, Yang Y and Zhang XL. B4GALT5 inhibits CD8(+) T-cell response by downregulating MHC-I level through ERAD pathway in PDAC. J Immunother Cancer 2025; 13: e010908.
[28] Tian P, Wei JX, Li J, Ren JK and Yang JJ. LncRNA SNHG1 regulates immune escape of renal cell carcinoma by targeting miR-129-3p to activate STAT3 and PD-L1. Cell Biol Int 2021; 45: 1546-1560.

[29] Prokhnevska N, Cardenas MA, Valanparambil RM, Sobierajska E, Barwick BG, Jansen C, Reyes Moon A, Gregorova P, delBalzo L, Greenwald R, Bilen MA, Alemozaffar M, Joshi S, Cimmino C, Larsen C, Master V, Sanda M and Kissick H. CD8(+) T cell activation in cancer comprises an initial activation phase in lymph nodes followed by effector differentiation within the tumor. Immunity 2023; 56: 107-124, e105.

[30] Chen C and Xu P. Cellular functions of cGAS-STING signaling. Trends Cell Biol 2023; 33: 630-648.

[31] Huang X, Yao J, Liu L, Chen J, Mei L, Huangfu J, Luo D, Wang X, Lin C, Chen X, Yang Y, Ouyang S, Wei F, Wang Z, Zhang S, Xiang T, Neculai D, Sun Q, Kong E, Tate EW and Yang A. S-acylation of p62 promotes p62 droplet recruitment into autophagosomes in mammalian autophagy. Mol Cell 2023; 83: 3485-3501, e3411.

[32] Hopfner KP and Hornung V. Molecular mechanisms and cellular functions of cGAS-STING signalling. Nat Rev Mol Cell Biol 2020; 21: 501-521.

[33] Prabakaran T, Bodda C, Krapp C, Zhang BC, Christensen MH, Sun C, Reinert L, Cai Y, Jensen SB, Skouboe MK, Nyengaard JR, Thompson CB, Lebbink RJ, Sen GC, van Loo G, Nielsen R, Komatsu M, Nejsum LN, Jakobsen MR, Gyrd-Hansen M and Paludan SR. Attenuation of cGAS-STING signaling is mediated by a p62/SQSTM1-dependent autophagy pathway activated by TBK1. EMBO J 2018; 37: e97858.

[34] Gui X, Yang H, Li T, Tan X, Shi P, Li M, Du F and Chen ZJ. Autophagy induction via STING trafficking is a primordial function of the cGAS pathway. Nature 2019; 567: 262-266.

[35] Wang Y, Wu S, Zhang X, Zheng W, Wang Z, Zhang J, Chen J and Wang H. cGAS-STING and autophagy: crosstalk, molecular mechanisms, and targeted therapy. Arch Toxicol 2025; 100: 145-172.

[36] Lu Q, Chen Y, Li J, Zhu F and Zheng Z. Crosstalk between cGAS-STING pathway and autophagy in cancer immunity. Front Immunol 2023; 14: 1139595.

[37] Schmid M, Fischer P, Engl M, Widder J, Kerschbaum-Gruber S and Slade D. The interplay between autophagy and cGAS-STING signaling and its implications for cancer. Front Immunol 2024; 15: 1356369.

[38] Ghosh M, Saha S, Bettke J, Nagar R, Parrales A, Iwakuma T, van der Velden AWM and Martinez LA. Mutant p53 suppresses innate immune signaling to promote tumorigenesis. Cancer Cell 2021; 39: 494-508, e495.

[39] Li W, Li K, Chen Y, Wang S, Xu K, Ye S, Zhao B, Yuan H, Li Z, Shen Y, Mou T, Wang Y, Zhou W and Ma W. IRF1 transcriptionally up-regulates CXCL10 which increases CD8(+) T cells infiltration in colorectal cancer. Int Immunopharmacol 2025; 144: 113678.

[40] Kang LP, Xu C, Xu P, Huang DH and Jiang ZB. Brazilin inhibits the proliferation of non-small cell lung cancer by regulating the STING/TBK1/IRF3 pathway. J Cell Mol Med 2025; 29: e70688.

[41] Tan Y, Zhu Q, Yang M, Yang F, Zeng Q, Jiang Z and Li D. Tetrandrine activates STING/TBK1/IRF3 pathway to potentiate anti-PD-1 immunotherapy efficacy in non-small cell lung cancer. Pharmacol Res 2024; 207: 107314.

[42] Zhang Z and Zhang C. Regulation of cGAS-STING signalling and its diversity of cellular outcomes. Nat Rev Immunol 2025; 25: 425-444.

[43] Kang LP, Xie H, Huang HJ, Xu P, Xu C, Huang DH and Jiang ZB. Pterostilbene inhibits non-small cell lung cancer progression by activating the STING pathway and enhancing antitumor immune response. Front Immunol 2025; 16: 1622284.